© 2019. Published by The Company of Biologists Ltd | Journal of Cell Science (2019) 132, jcs222331. doi:10.1242/jcs.222331

RESEARCH ARTICLE

BBS4 is required for intraflagellar transport coordination and basal body number in mammalian olfactory cilia

Cedric R. Uytingco[1,2], Corey L. Williams[1,2], Chao Xie[1,2], Dana T. Shively[1,2], Warren W. Green[1,2], Kirill Ukhanov[1,2], Lian Zhang[1,2], Darryl Y. Nishimura[3], Val C. Sheffield[3,4] and Jeffrey R. Martens[1,2,*]

ABSTRACT

Bardet–Beidl syndrome (BBS) manifests from genetic mutations encoding for one or more BBS proteins. BBS4 loss impacts olfactory ciliation and odor detection, yet the cellular mechanisms remain unclear. Here, we report that *Bbs4*$^{-/-}$ mice exhibit shorter and fewer olfactory sensory neuron (OSN) cilia despite retaining odorant receptor localization. Within *Bbs4*$^{-/-}$ OSN cilia, we observed asynchronous rates of IFT-A/B particle movements, indicating miscoordination in IFT complex trafficking. Within the OSN dendritic knob, the basal bodies are dynamic, with incorporation of ectopically expressed centrin-2 and γ-tubulin occurring after nascent ciliogenesis. Importantly, BBS4 loss results in the reduction of basal body numbers separate from cilia loss. Adenoviral expression of BBS4 restored OSN cilia lengths and was sufficient to re-establish odor detection, but failed to rescue ciliary and basal body numbers. Our results yield a model for the plurality of BBS4 functions in OSNs that includes intraciliary and periciliary roles that can explain the loss of cilia and penetrance of ciliopathy phenotypes in olfactory neurons.

KEY WORDS: Olfactory cilia, Bardet–Biedl syndrome, Peripheral olfactory system, Intraflagellar transport, Basal body, Gene therapy

INTRODUCTION

Bardet–Beidl syndrome (BBS) is a ciliopathy in which symptoms manifest from disruptions in ciliary growth, maintenance and/or function. BBS is a pleiotropic disease but its penetrance can vary between ciliated tissues. Patients with BBS exhibit numerous clinical manifestations including olfactory dysfunction (Kulaga et al., 2004; May-Simera et al., 2009; Mykytyn et al., 2001; Nishimura et al., 2004; Riise et al., 2002). Evidence of olfactory dysfunctions resulting from BBS have been identified across multiple patient populations and animal models (Kulaga et al., 2004; McIntyre et al., 2012; Mykytyn et al., 2004; Nishimura et al., 2004; Tadenev et al., 2011; Williams et al., 2017). The disease is an autosomal recessive disorder resulting from homozygous or compound heterozygous mutations in genes that code for proteins that assemble or associate with the BBSome protein complex. To date, 21 BBS genes (*BBS1–BBS21*) have been identified, all linked to diseases in patients (Aldahmesh et al., 2014; Heon et al., 2016; Khan et al., 2016; Lindstrand et al., 2016; Loktev et al., 2008; Nachury et al., 2007; Scheidecker et al., 2014). Composed of eight BBS proteins (1, 2, 4, 5, 7, 8, 9, 18), the BBSome complex is postulated to function as a membrane coat complex that associates with other proteins in intraflagellar transport (IFT), driving ciliary biogenesis and regulating the ciliary trafficking of receptors and other transmembrane proteins (Berbari et al., 2008; Domire et al., 2011; Jin et al., 2010; Lechtreck et al., 2009; Liu and Lechtreck, 2018; Loktev and Jackson, 2013; Pan et al., 2006; Seo et al., 2011; Xu et al., 2015).

IFT is an evolutionarily conserved protein trafficking system that functions by a process in which macromolecular protein 'trains' consisting of IFT-A and IFT-B subcomplexes bidirectionally traverse the ciliary microtubule axoneme via association with kinesin and dynein motors (Rosenbaum and Witman, 2002). The continuous and coordinated movement of proteins along the ciliary microtubule axoneme is essential for cilium formation and maintenance. Previous work from our laboratory identified BBSome proteins as bona fide constituents of IFT in olfactory sensory neurons (OSNs) (Williams et al., 2014). In BBS mutant mice, OSNs lack the capacity to build/maintain cilia, rendering the cells incapable of odor detection. However, the precise role of BBSome protein constituents in OSN cilia formation or maintenance is unclear.

In OSNs, ciliogenesis occurs following centriole duplication and migration to the dendritic knob at the apical surface of the olfactory epithelium (OE). In the dendritic knob, centrioles are converted to basal bodies and anchored to the plasma membrane. The basal body serves as the microtubule organizing center (MTOC) in the dendritic knob for the ciliary axoneme (Burton, 1992), as well as a nucleation site for microtubules that project from the dendritic knob back through the dendritic shaft toward the cell body (Burton and Laveri, 1985). Early evidence from the ciliated protist *Tetrahymena thermophila* suggests that basal body components can be dynamic, especially during initial assembly (Bayless et al., 2016; Pearson et al., 2009). However, the exact incorporation or association of the basal body components within mammalian OSNs is unknown.

BBS4 is suggested to play a role in both cilia maintenance and microtubule anchoring of centrioles. BBS4 is the last protein component to be incorporated into the BBSome complex and loss-of-function mutations of BBS4 constitute a signification cause of BBS (Billingsley et al., 2011; Zhang et al., 2012). BBS4 plays multiple roles within the cilia, including regulating the trafficking of transmembrane proteins, including G-protein-coupled receptors (GPCR), into the cilia (Berbari et al., 2008) and export of receptors out of the cilia (Xu et al., 2015). Besides playing a ciliary role, BBS4 has extraciliary functions, including acting as an adaptor protein for shuttling cargo to the pericentriolar region to regulate cell cycle progression and microtubule organization in dividing cells

[1]Department of Pharmacology and Therapeutics, Gainesville, FL 32610, USA. [2]Center for Smell and Taste, University of Florida College of Medicine, Gainesville, FL 32610, USA. [3]Department of Pediatrics, University of Iowa, Iowa City, IA 52242, USA. [4]Howard Hughes Medical Institute, University of Iowa, Iowa City, IA 52242, USA.

*Author for correspondence (martensj@ufl.edu)

C.R.U., 0000-0003-1625-3988; K.U., 0000-0003-0633-9067; J.R.M., 0000-0002-0451-2703

Received 9 July 2018; Accepted 11 January 2019

Journal of Cell Science (2019) 132, jcs222331. doi:10.1242/jcs.222331

(Gascue et al., 2012; Gerdes et al., 2007; Kim et al., 2004; Leitch and Zaghloul, 2014; Prieto-Echagüe et al., 2017; Stawicki et al., 2016). However, the role of BBS4 at basal bodies in terminally differentiated cells such as neurons has not been shown. Previous work in OSNs has shown that microtubule disorganization and protein mislocalization occurred at the apical surface of the OE with loss of BBS4, but how this was connected to the loss of cilia was not elucidated (Kulaga et al., 2004). In the present study, we show that loss of BBS4 results in a dramatic reduction of cilia length and number from individual OSNs, and show, for the first time, a corresponding loss of basal bodies. Contrary to the loss of BBS1 in OSNs (Williams et al., 2017), loss of BBS4 did not affect BBSome protein entry into the cilia. However, BBS4 deficiency resulted in a miscoordination of IFT-A and IFT-B subcomplexes in OSN cilia, as measured by alterations in IFT122 and IFT88 anterograde and retrograde trafficking velocities. Following intranasal delivery to OSNs of an adenoviral construct containing the wild-type *Bbs4* gene, we observed restoration of cilia lengths, but not cilia or basal body number. Interestingly, restoration of cilia length in a subset of OSNs was sufficient to recover olfactory function at the periphery. Together, these observations demonstrated previously unknown mechanisms of OSN cilia shortening and cilia number loss resulting from BBS4 loss, and highlight the capacity of vector-mediated gene replacement to restore ciliation and rescue olfactory function in a model of BBS disease.

RESULTS

Loss of BBS4 reduces cilia within cells of the olfactory epithelium

In order to understand the penetrance and pathogenic mechanism within the olfactory system of *Bbs4* global knockout (*Bbs4*$^{-/-}$) mice, we first evaluated ciliation within the OE. At the apical surface, cilia extend from the OSN dendritic knob toward the lumen of the nasal cavity, where odorants from the external environment are readily accessible. Immunostaining for acetylated α-tubulin, a post-translational modification of ciliary microtubules in wild-type animals, robustly lined the apical surface of control mice OE (Fig. 1A,B). On the other hand, *Bbs4*$^{-/-}$ mice demonstrated a more than 50% reduction [t(291)=19.6, P<0.0001, unpaired *t*-test] in apical acetylated α-tubulin immunolabeling (Fig. 1C,D,I). Despite loss of ciliation, the *Bbs4*$^{-/-}$ mutant OE did not exhibit significant differences in OE thicknesses [t(104)=1.472, P=0.1440, unpaired *t*-test] and olfactory marker protein (OMP)-positive neuronal counts [t(49)=1.357, P=0.1811, unpaired *t*-test] when compared with controls (Fig. S1A,B). Examination of younger, postnatal 5-day-old *Bbs4*$^{-/-}$ mutant mice demonstrated similar loss of OE ciliation (Fig. S2). However, certain regions retained acetylated α-tubulin immunolabeling at the apical surface, suggesting OE ciliary degradation as the *Bbs4*$^{-/-}$ mutant mice ages. Although the OE cilia are dramatically lost, the motile cilia of the respiratory epithelium (RE) were not affected in *Bbs4*$^{-/-}$ mice, demonstrating robust apical acetylated α-tubulin immunolabeling (Fig. 1B,D; Fig. S1C,D).

To substantiate whether reduced acetylated α-tubulin immunolabeling in *Bbs4*$^{-/-}$ mutant mice corresponds to individual OSN cilia loss, we performed scanning electron microscopy (SEM) of the OE. The cilia layer that normally exists across the surface of the OE was severely diminished in *Bbs4*$^{-/-}$ mutant mice, exposing the underlying supporting cells, but retained the capacity to build residual cilia (Fig. 1E,F). In order to examine the residual cilia of individual *Bbs4*$^{-/-}$ OSNs in higher resolution, we utilized a combination of adenoviral-mediated ectopic expression of fluorescently tagged ciliary markers and live *en face* confocal imaging of the intact OE (Williams et al., 2014). Using an inert lipid-anchored fluorophore (myristoylated-palmitoylated-mCherry; MP-mCh), which labels the inner leaflet of the plasma membrane (Fig. 1G,H), *Bbs4*$^{-/-}$ mutant OSNs demonstrated shorter [mean length=6.2±0.3 µm per OSN; t(111)=11.64, P<0.0001, unpaired *t*-test] and fewer [mean number=10.9±0.4 cilia per OSN; t(111)=14.1, P<0.0001, unpaired *t*-test] cilia compared with control mice (25.5±2.7 µm per OSN and 24.4±0.9 cilia per OSN, respectively) (Fig. 1J–L). In addition to the reduced cilia length and number, some *Bbs4*$^{-/-}$ mutant OSNs demonstrated swellings at the distal ciliary tip (Fig. S3).

Recent work has shown that OSNs are one of two populations of ciliated cells in the OE (Joiner et al., 2015). Besides OSNs, the *Bbs4*$^{-/-}$ mice demonstrated a reduction in primary cilia on horizontal basal cells (HBCs), the neuronal stem cell population near the basal lamina that is important for regeneration of the OE (Joiner et al., 2015). Immunostaining for cytokeratin-5 (K5; also known as Krt5) and Arl13b, markers for HBCs and primary cilia, respectively, demonstrated a 30% decrease in the number of ciliated HBCs [t(64)=5.0, P<0.0001, unpaired *t*-test] without a change in total HBC number [t(22)=0.003, P=0.998, unpaired *t*-test] (Fig. S4A–C). Consistent with the reduction in ciliated HBCs (Joiner et al., 2015), *Bbs4*$^{-/-}$ mutant mice exhibited reduced regenerative capacity following methimazole (MMZ)-mediated OE ablation with diminished OMP-positive cells (Fig. S4D) and reduced OE thicknesses [47.1±1.3 µm; F(3382)=49.91, P<0.0001, one-way ANOVA, Tukey post hoc] compared with ablated control mice (59.8 ±1.4 µm), sham control mice (68.1±1.4 µm) and *Bbs4*$^{-/-}$ mutant mice (68.2±1.5 µm) (Fig. S4E). Together, these observations show the loss of both cilia length and number in individual *Bbs4*$^{-/-}$ OSNs, as well as penetrance of the *Bbs4*$^{-/-}$ phenotype to the HBC population.

Bbs4$^{-/-}$ mutants retain the capacity for trafficking of odorant receptors and other signaling proteins to the cilia of OSNs

Previous studies have implicated BBSome components in the trafficking of transmembrane proteins, including GPCRs, into the cilia (Abd-El-Barr et al., 2007; Berbari et al., 2008; Jin et al., 2010; Leitch and Zaghloul, 2014; Loktev and Jackson, 2013; Loktev et al., 2008; Starks et al., 2015; Ye et al., 2018). Specific to BBS4, *Bbs4*$^{-/-}$ mice demonstrated mislocalization and perturbance of phototransduction proteins in photoreceptor cells (Nishimura et al., 2004). In addition, BBS4 was specifically implicated in the membrane trafficking of insulin receptors (Starks et al., 2015), and the ciliary trafficking of GPCRs and ion channels (Xu et al., 2015). In the olfactory system, deletion of BBS4 resulted in a decrease in the intensity of antibody labeling at the apical surface of the OE for adenylyl cyclase III (ACIII) and $G_{\gamma 13}$ (Kulaga et al., 2004). Here, we confirmed that the immunoreactivities for endogenous ACIII and cyclic nucleotide-gated channel alpha 2 (CNGA2) were decreased at the OE apical surfaces of *Bbs4*$^{-/-}$ mutant mice, corresponding with the reduction in acetylated α-tubulin immunostaining (Fig. 2A,B). In addition, we extend the analysis to show that endogenous levels of mOR28 (also known as Olfr1507) odorant receptor were also diminished at the apical surface (Fig. 2C). Although it showed a decrease, the cross-sectional analysis could not accurately distinguish between the dendritic knob or residual cilia. In order to examine ciliary localization under higher resolution and test the potential mechanism of altered protein trafficking into OSN cilia, we ectopically expressed, in differentiated OSNs, fluorescently tagged signaling proteins together with the full-length cilia

Journal of Cell Science (2019) 132, jcs222331. doi:10.1242/jcs.222331

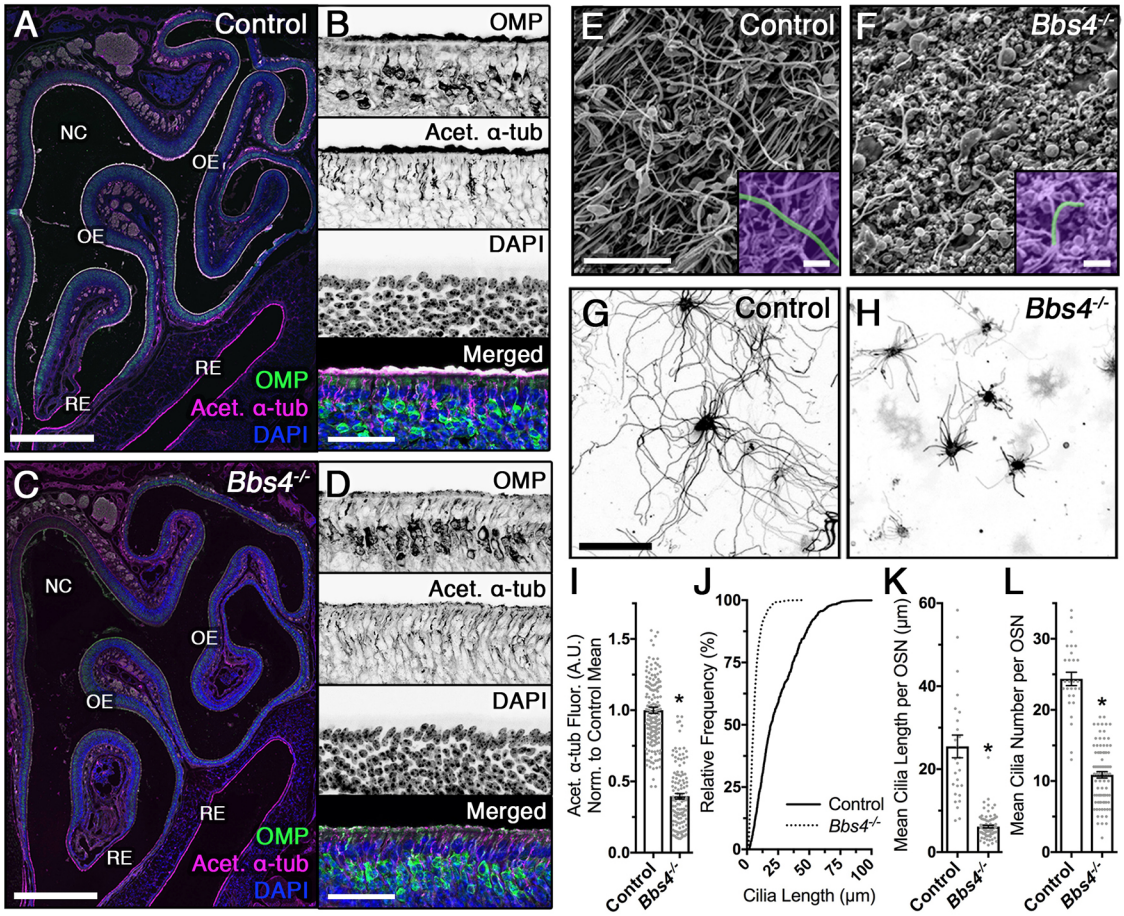

Fig. 1. Reduced cilia length and number in *Bbs4*$^{-/-}$ mutant mice. (A,C) Representative global confocal images of coronal sections through nasal epithelium of control (A) and *Bbs4*$^{-/-}$ mutant (C) mice, immunostained for olfactory marker protein (OMP) and acetylated α-tubulin (Acet. α-tub) to visualize mature olfactory sensory neurons (OSNs) and ciliary microtubules. Coronal sections depict the nasal cavity (NC) lined with the olfactory epithelium (OE) and respiratory epithelium (RE). (B,D) Representative OE of control (B) and *Bbs4*$^{-/-}$ mutant (D) mice, immunostained for OMP (top), Acet. α-tub (second from top), DAPI (second from bottom) and merged (bottom). (E,F) Representative scanning electron micrographs of the OE surface in control (E) and *Bbs4*$^{-/-}$ mutant (F) mice. (G,H) Representative live *en face* confocal images of ectopically expressing myristoylated-palmitoylated-mCherry (MP-mCh) in OSN cilia of control (G) and *Bbs4*$^{-/-}$ mutant (H) mice. (I) Quantified data showing a significant reduction in Acet. α-tub in *Bbs4*$^{-/-}$ mutants (0.4±0.02 a.u.; n=9 mice) compared with control mice (1.0±0.02 a.u.; n=8 mice) [t(291)=19.6, *P<0.0001, unpaired t-test]. (J) Cumulative distribution of overall cilia lengths from wild-type control (solid line; n=995 cilia from 28 OSNs) and *Bbs4*$^{-/-}$ (dotted line; n=978 cilia from 85 OSNs) mice, measured from live *en face* confocal images. (K) Mean cilia length per OSN was lower in *Bbs4*$^{-/-}$ mutants (6.2±0.3 µm per OSN; n=85 OSNs) compared with controls (25.5±2.7 µm per OSN; n=28 OSNs) [t(111)=11.64, *P<0.0001, unpaired t-test]. (L) Cilia number per OSN was lower in *Bbs4*$^{-/-}$ mutants (10.9±0.4 cilia per OSN; n=85 OSNs) compared with controls (24.4±0.9 cilia per OSN; n=28 OSNs) [t(111)=14.1, *P<0.0001, unpaired t-test]. Values represent means±s.e.m. Scale bars: 500 µm (A,C), 40 µm (B,D), 2.5 µm (E,F), 1.25 µm (insets in E,F), 20 µm (G).

marker, MP-GFP/mCh. Visualized using live *en face* confocal imaging, *Bbs4*$^{-/-}$ mutants retained the capacity for ciliary trafficking of fluorescently tagged adenylyl cyclase III (ACIII-GFP) and the cyclic nucleotide-gated channel B1 subunit (CNGB1-mCh), which is necessary for ciliary targeting of olfactory CNG channels (Jenkins et al., 2006; Michalakis et al., 2006) (Fig. 2D). To examine the impact of BBS4 loss on the ciliary entry of GPCRs, we ectopically expressed mCherry-tagged M71 odorant receptor (mCh-M71) with MP-GFP in *Bbs4*$^{-/-}$ mutant mice (Fig. 2D). The mCh-M71 receptor localized to the dendritic knob and, importantly, the cilia of *Bbs4*$^{-/-}$ OSNs. The continual presence of the GPCR was further supported by *en face-en bloc* immunostaining of endogenous M71/72 odorant receptors in *Bbs4*$^{-/-}$ OE (Fig. 2E). Together, these observations show that, unlike other ciliated cell types, *Bbs4*$^{-/-}$ mutant OSNs retain the capacity for olfactory signaling protein and odorant receptor trafficking to the cilia.

BBS4$^{-/-}$ mutants show alterations in IFT-A/B trafficking velocities and particle numbers

The presence of residual OSN cilia permitted an examination of the dynamic trafficking and intraflagellar transport mechanisms within *Bbs4*$^{-/-}$ mutant mice. In order to examine BBS and IFT protein entry and intraciliary movement in *Bbs4*$^{-/-}$ OSN cilia, we performed live *en face* total internal reflection fluorescence microscopy (TIRFm) on OSNs ectopically expressing either fluorescently tagged BBSome proteins (BBS2-GFP, BBS3/Arl6-GFP, BBS5-GFP) or IFT proteins (IFT122-GFP, IFT88-GFP). From these experiments, we found that BBSome protein (BBS2, BBS3, BBS5) entry into the residual cilia of *Bbs4*$^{-/-}$ mutant mice was unaffected (Fig. 3A,B). Closer examination of the bidirectional transport of the BBSome complex showed that BBS5-GFP anterograde movement was unchanged [t(191)=1.51, P=0.132, unpaired t-test], but there was an increase in retrograde trafficking velocity [t(151)=4.29, P<0.0001, unpaired t-test] between control

Journal of Cell Science (2019) 132, jcs222331. doi:10.1242/jcs.222331

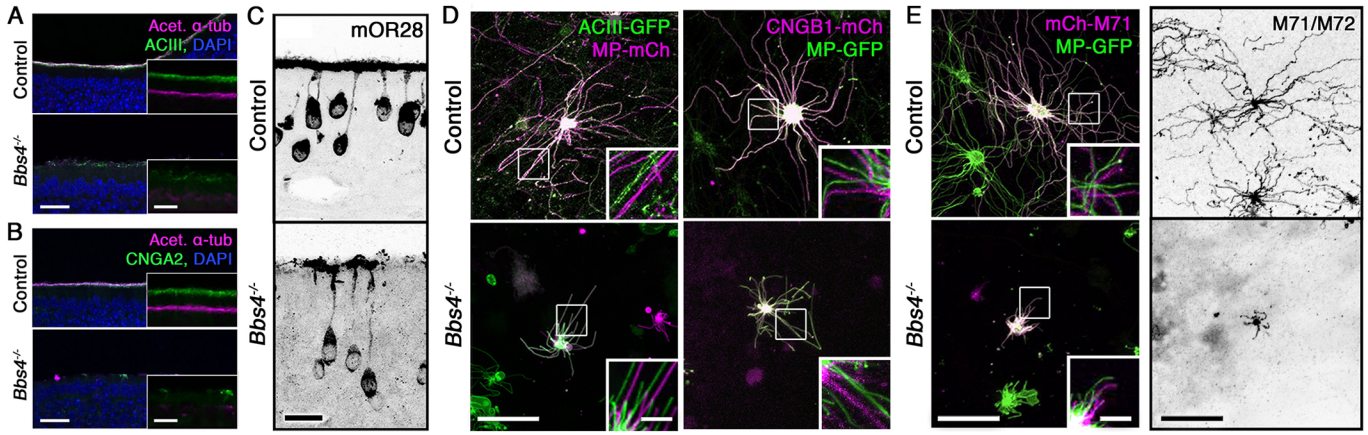

Fig. 2. *Bbs4*$^{-/-}$ mutant mice retain ciliary and signaling protein trafficking. (A) Representative confocal images of coronal sections through OE of control (top) and *Bbs4*$^{-/-}$ mutant (bottom) mice, immunostained for acetylated α-tubulin (Acet. α-tub) and adenylyl cyclase III (ACIII). Insets show zoomed-in offset views of individual immunolabeling. (B) Coronal sections through OE of control (top) and *Bbs4*$^{-/-}$ mutant (bottom) mice, immunostained for Acet. α-tub and cyclic nucleotide-gated channel alpha 2 (CNGA2). Insets show zoomed-in offset views of individual immunolabeling. (C) Representative coronal section of endogenous mOR28 odorant receptor localization in control (top) and *Bbs4*$^{-/-}$ mutant (bottom) OSNs. (D) Representative *en face* confocal microscopy images of ectopically expressing ACIII-GFP (left) and CNGB1-mCh (right) in control (top) and *Bbs4*$^{-/-}$ mutant (bottom) OSNs co-expressed with a lipid-anchored fluorophore (MP-mCh/GFP). Insets show zoomed-in views of individual cilia with labeled proteins color offset. (E) Representative *en face* images of ectopically expressed mCh-M71 with MP-GFP (left) and endogenous M71/M72 (right) odorant receptors in control (top) and *Bbs4*$^{-/-}$ mutant (bottom) OSNs. Insets show zoomed-in views of individual cilia with labeled proteins color offset. Scale bars: 20 µm (A,B), 10 µm (insets in A,B), 10 µm (C), 20 µm (D,E), 5 µm (insets in D,E).

and *Bbs4*$^{-/-}$ OSN cilia (Fig. 3B,C). We then extended our observation to examine specifically the bidirectional transport of IFT-A and IFT-B subcomplexes, as measured by the ciliary distribution and movement of IFT122 and IFT88, respectively (Fig. 3D,G). In the residual cilia of *Bbs4*$^{-/-}$ mutant OSNs, the anterograde and retrograde IFT122-GFP trafficking velocities remained unchanged from control [anterograde, $F(21435)=32.65$, $P<0.0001$, one-way ANOVA, Tukey post hoc, $P=0.999$; retrograde, $F(21165)=82.13$, $P<0.0001$, one-way ANOVA, Tukey post hoc, $P=0.2108$] (Fig. 3E). However, IFT88-GFP demonstrated a twofold increase in the rate of anterograde [$F(21184)=422.1$, $P<0.0001$, one-way ANOVA, Tukey post hoc, $P<0.0001$] and retrograde [$F(2871)=360$, $P<0.0001$, one-way ANOVA, Tukey post hoc, $P<0.0001$] movement in *Bbs4*$^{-/-}$ mutant OSNs (Fig. 3H). The alteration in trafficking velocities denotes a BBS4-dependent decoupling of the IFT complex and suggests that the BBSome cargo impacts the velocity of IFT transport. If true, we hypothesized that, in the absence of the BBSome as cargo, velocities of both IFT-A and IFT-B particles would increase in the anterograde and retrograde directions. To further test this, we extended our observations to the OSN-specific knockout of *Bbs1* (*Bbs1* KO), where the BBSome fails to enter the OSN cilia (Williams et al., 2017). Similar to *Bbs4*$^{-/-}$ OSNs, we observed increased anterograde ($P>0.0001$) and retrograde ($P<0.0001$) trafficking velocities of IFT88-GFP in *Bbs1* KO OSNs, and also increased IFT122-GFP anterograde ($P<0.0001$) and retrograde ($P<0.0001$) trafficking (Fig. 3E,H; Fig. S5). In addition to alterations in individual IFT particle trafficking velocities, *Bbs4*$^{-/-}$ mutant OSNs demonstrated a near twofold increase in anterograde [$t(82)=2.55$, $P=0.0125$, unpaired *t*-test] and retrograde [$t(82)=1.37$, $P=0.05$, unpaired *t*-test] IFT122-GFP particle frequencies compared with wild-type controls (Fig. 3F). Similarly, an increase in anterograde [$t(195)=7.66$, $P<0.0001$, unpaired *t*-test] and retrograde [$t(195)=4.73$, $P<0.001$, unpaired *t*-test] IFT88-GFP particle frequencies was observed (Fig. 3I). Together, these data suggest that BBS4 and the BBSome are involved in the coordination and particle frequency of IFT-A and IFT-B subcomplexes for proper IFT motor movement in OSN cilia.

Loss of BBS4 causes reduction in basal body number

The basal body acts as a nucleation site for axoneme extension during ciliogenesis, orientation of the cilium and protein entry selectivity (Marshall, 2008). Work from *T. thermophila* has demonstrated that protein incorporation into basal bodies is dynamic during initial cilia assembly, with the degree of exchange dependent on the identity of the protein (Pearson et al., 2009). Previous studies have shown the interaction between BBS4 and the basal body proteins (Chamling et al., 2014; Kim et al., 2004). To explore the dynamics of protein exchange and understand the impact of BBS4 loss on basal body stability in OSNs, we imaged, by *en face* confocal microscopy, the incorporation of two distinct canonical basal body markers in the dendritic knobs of wild-type and *Bbs4*$^{-/-}$ mice. Ectopic expression of GFP-centrin-2 and γ-tubulin-mCh shows colocalization to basal bodies at the base of cilia of terminally differentiated OSNs (Fig. 4A). Using mCh-centrin-2 puncta within the dendritic knob as a marker, examination of basal body number revealed a reduction in *Bbs4*$^{-/-}$ mutant OSNs (17.7±0.7 basal bodies per OSN) compared with controls (22.5±0.6 basal bodies per OSN) [$t(129)=4.66$, $P<0.0001$, unpaired *t*-test] (Fig. 4B,C). In addition, some basal bodies in *Bbs4*$^{-/-}$ mutant OSNs did not associate with individual cilia, unlike the basal bodies from control OSNs. In order to determine whether basal body loss was a generalized consequence of the failure to maintain cilia, we extend our observation to mice with an OSN-specific knockout of IFT88 (*Ift88* KO), which demonstrated a near complete loss of OSN cilia (Green et al., 2018). Despite the severe loss of ciliation, *Ift88* KO mice did not exhibit reductions in basal body numbers (20.9±0.3 basal bodies per OSN) compared with littermate controls (20.1±0.2 basal bodies per OSN) [$t(401)=1.9$, $P=0.058$, unpaired *t*-test] (Fig. 4D,E) Together, these observations suggest that ciliary and basal body loss are not concurrent, and that loss of the

Journal of Cell Science (2019) 132, jcs222331. doi:10.1242/jcs.222331

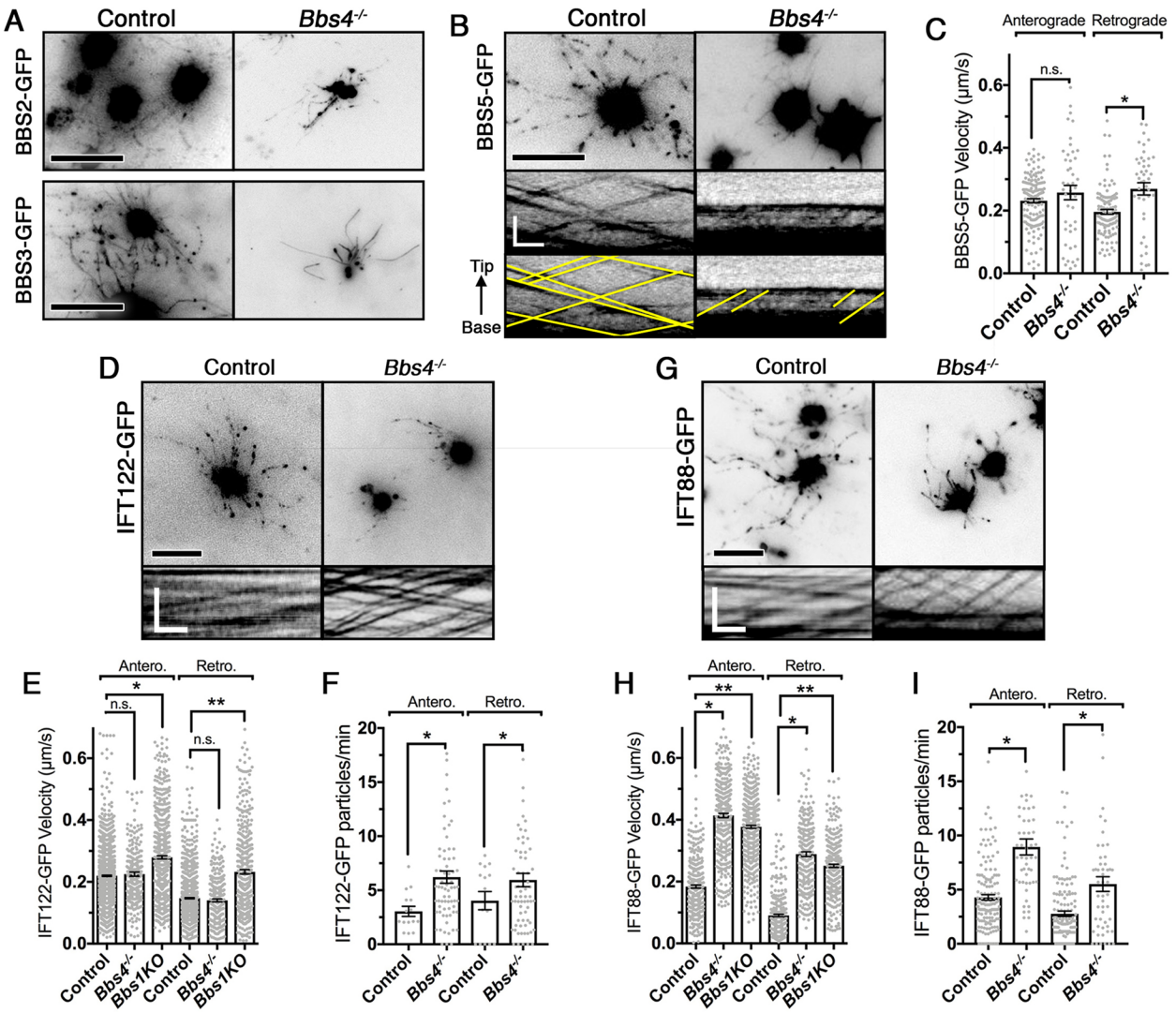

Fig. 3. *Bbs4*$^{-/-}$ OSNs exhibit alterations in IFT-A/B trafficking velocities and particle numbers. (A,B) Representative *en face* TIRFm images of ectopically expressing GFP-tagged BBS2, BBS3 and BB5 proteins in control (left) and *Bbs4*$^{-/-}$ mutant (right) OSNs. (B, bottom) Representative kymogram of BBS5-GFP from control (left) and *Bbs4*$^{-/-}$ mutant (right) OSNs. (C) BBS5-GFP anterograde trafficking velocities were unchanged between controls (0.232±0.007 µm/s; *n*=148 cilia) and *Bbs4*$^{-/-}$ mutants (0.232±0.007 µm/s; *n*=45 cilia) [t(191)=1.51, n.s., *P*=0.132, unpaired *t*-test], while retrograde trafficking velocities were higher in *Bbs4*$^{-/-}$ mutants (0.232±0.007 µm/s; *n*=44 cilia) compared with controls (0.232±0.007 µm/s; *n*=109 cilia) [t(151)=4.29, **P*<0.0001, unpaired *t*-test]. (D,G) Representative *en face* TIRFm images of ectopically expressed IFT122-GFP (D) and IFT88-GFP (G) in control (left) and *Bbs4*$^{-/-}$ (right) mice. (E,H) Quantification of anterograde and retrograde trafficking velocities of IFT122-GFP (E) and IFT88-GFP (H) from wild-type control, *Bbs4*$^{-/-}$ and *Bbs1* KO OSN cilia. (E) *Bbs4*$^{-/-}$ OSNs demonstrate unchanged anterograde (0.225±0.007 µm/s; *n*=301 cilia) and retrograde (0.140±0.004 µm/s; *n*=283 cilia) IFT122-GFP trafficking velocities compared with control OSNs (anterograde: 0.225±0.006 µm/s; *n*=1805 cilia; retrograde: 0.154±0.004 µm/s; *n*=1455 cilia). However, *Bbs1* KO OSNs demonstrated increased anterograde (0.280±0.005 µm/s; *n*=647 cilia) and retrograde (0.232±0.007 µm/s; *n*=431 cilia) IFT122-GFP trafficking [anterograde, *F*(21435)=32.65, *P*<0.0001, one-way ANOVA, Tukey post hoc, n.s., *P*=0.999, **P*<0.0001; retrograde, *F*(21165)=82.13, *P*<0.0001, one-way ANOVA, Tukey post hoc, n.s., *P*=0.2108, ***P*<0.0001]. (H) *Bbs4*$^{-/-}$ and *Bbs1* KO OSNs demonstrate increased anterograde (0.414±0.007 µm/s; *n*=361 cilia; 0.377±0.005 µm/s; *n*=510 cilia) and retrograde (0.289±0.008 µm/s; *n*=247 cilia; 0.251±0.005 µm/s; *n*=323 cilia) IFT88-GFP trafficking velocities compared with control OSNs (0.184 ±0.005 µm/s; *n*=316 cilia and 0.090±0.004 µm/s; *n*=304 cilia, respectively) [anterograde, *F*(21184)=422.1, *P*<0.0001, one-way ANOVA, Tukey post hoc, **P*<0.0001, ***P*<0.0001; retrograde, *F*(2871)=360, *P*<0.0001, one-way ANOVA, Tukey post hoc, **P*<0.0001, ***P*<0.0001]. (F,I) Quantification of anterograde and retrograde IFT122-GFP (F) and IFT88-GFP (I) particle frequencies from control and *Bbs4*$^{-/-}$ mutant OSNs. (F) *Bbs4*$^{-/-}$ mutant OSNs exhibited increased IFT122-GFP anterograde [6.22±0.56 particles/min; *n*=69 cilia; t(82)=2.55, **P*=0.0125, unpaired *t*-test] and retrograde [5.95±0.62 particles/min; *n*=69 cilia; t(195)=4.73, **P*<0.001, unpaired *t*-test] particle frequencies compared with controls (anterograde, 3.05±0.46 particles/min; *n*=30 cilia; retrograde, 4.04±0.85 particles/min; *n*=30 cilia). (I) *Bbs4*$^{-/-}$ mutant OSNs exhibited increased IFT88-GFP anterograde [8.94±0.74 particles/min; *n*=51 cilia; t(195)=7.66, **P*<0.0001, unpaired *t*-test] and retrograde [5.51±0.67 particles/min; *n*=51 cilia; t(195)=4.73, **P*<0.001, unpaired *t*-test] particle frequencies compared with controls (anterograde, 4.28±0.25 particles/min; *n*=146 cilia; retrograde, 2.77±0.25 particles/min; *n*=146 cilia). Scale bars: 10 µm (A,B,D,G), 5 s×5 µm (kymogram in B), 10 s×5 µm (kymogram in D,G).

cilia alone does not preclude basal body loss. Overall, our results demonstrate that *Bbs4*$^{-/-}$ mutants retain the capacity to assemble basal bodies in OSNs but fail to maintain normal basal body number.

Ectopically expressed BBS4 rescues cilia length, but not cilia and basal body numbers

To assess the capacity for re-expression of wild-type BBS to rescue OSN cilia phenotypes, we adenovirally expressed wild-type BBS4

Journal of Cell Science (2019) 132, jcs222331. doi:10.1242/jcs.222331

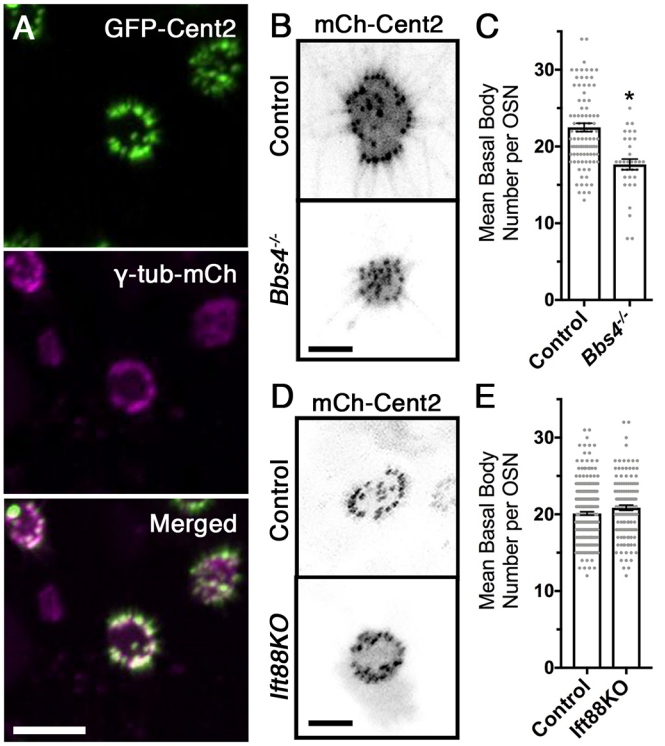

Fig. 4. Reduced basal body number in *Bbs4*$^{-/-}$ mutant mice. (A) Representative confocal *en face* images of GFP-centrin-2 (GFP-Cent2) and γ-tubulin-mCherry (γ-tub-mCh) colocalizing within the basal bodies of the OSN dendritic knob. (B) Representative images from control (top) and *Bbs4*$^{-/-}$ (bottom) OSNs co-infected with mCh-centrin-2 (mCh-Cent2) and MP-GFP, depicting loss of the ciliation corresponding to loss in basal bodies. (C) Quantification of basal body numbers demonstrated a decrease in *Bbs4*$^{-/-}$ OSNs (17.7±0.7 basal bodies per OSN; *n*=33 OSNs) compared with controls (22.5±0.6 basal bodies per OSN; *n*=98 OSNs) [t(129)=4.66, **P*<0.001, unpaired *t*-test]. (D) Representative confocal *en face* images of OSN dendritic knobs ectopically expressing mCh-Cent2 in control and *Ift88* KO mice. (E) Quantification of basal body number does not show a difference between control (20.1±0.2 basal bodies per OSN; *n*=268 OSNs) and *Ift88* KO (20.9±0.3 basal bodies per OSN; *n*=135 OSNs) [t(401)=1.9, *P*=0.058, unpaired *t*-test] mice. Scale bars: 5 µm (A), 2.5 µm (B,D).

(AV-BBS4-GFP) in *Bbs4*$^{-/-}$ mutant mice. Intranasal delivery of genetic material was shown to infect mature OSNs (Green et al., 2018; McIntyre et al., 2012; Williams et al., 2017). Mice [postnatal day (P) 8–11] were intranasally treated with three separate doses of 20 µl of AV-BBS4-GFP across three consecutive days, and tissues were examined or harvested 10 days later (P21–25). Treated *Bbs4*$^{-/-}$ mutant mice demonstrated increased acetylated α-tubulin intensities at the apical surface projecting from the corresponding dendrites of BBS4-GFP-positive *Bbs4*$^{-/-}$ OSNs (Fig. 5A, arrowheads), but not in the neighboring GFP-negative neurons. Examination of treated mice estimated an infection rate of 41.7±3.7 cells/mm (*n*=6 mice; mean±s.e.m.) of OE. Live *en face* TIRFm showed the capacity of ectopically expressed BBS4-GFP to undergo anterograde and retrograde IFT trafficking within *Bbs4*$^{-/-}$ mutant OSNs (Fig. 5B). In addition, live *en face* confocal imaging of *Bbs4*$^{-/-}$ mutant mice treated with BBS4-GFP and MP-mCh demonstrated partial restoration of mean ciliary lengths per OSN (18.2±1.8 µm per OSN) (Fig. 5C, arrowheads, D,E) compared with untreated OSNs from the same animal (6.87±0.6 µm per OSN) [$F(2,61)=83.95$, $P<0.0001$, one-way ANOVA, Tukey post hoc, $P<0.0001$] (Fig. 5C, inset, D,E) . However, cilia numbers were not restored in treated (12.7±1.2 cilia per OSN) versus untreated (11.1 ±0.7 cilia per OSN) *Bbs4*$^{-/-}$ OSNs [$F(2,61)=16.96$, $P<0.0001$, one-way ANOVA, Tukey post hoc, $P=0.5281$] (Fig. 5D–F). Similarly, ectopic expression of wild-type BBS4 did not restore basal body numbers (17.4±0.8 basal bodies per OSN) compared with untreated OSNs (14.8±0.8 basal bodies per OSN) [$F(2110)=24.61$, $P<0.0001$, one-way ANOVA, Tukey post hoc, $P=0.0933$] (Fig. 5G,H). Despite restoration of ciliary lengths, the inability to restore cilia and basal body number in mature OSNs emphasizes the role of BBS4 in cilia and basal body biogenesis; thus, limiting rescue to pre-existing cilia on mature OSNs.

Partial restoration of cilia length is sufficient for functional rescue

Previous reports show that loss of BBS4 results in olfactory dysfunctions in animals and patients (Iannaccone et al., 2005; Kulaga et al., 2004). We asked whether the partial restoration of cilia length, but not numbers, was sufficient to restore odor detection. In order to measure the functional effects on odor detection in *Bbs4*$^{-/-}$ mutant and rescued mice, we performed electro-olfactogram (EOG) recordings to examine the odor-evoked field potential responses on the surface of the OE. Compared with untreated *Bbs4*$^{-/-}$ mutants, *Bbs4*$^{-/-}$ mice receiving AV-BBS4-GFP showed significantly larger odor-evoked responses to increasing concentrations of amyl acetate (AA), 10^{-3} M 1-octanol (1-Oct) and 10^{-3} M hexanal (Hex) [$F(2346)=52.1$, $P<0.0001$, two-way ANOVA, Tukey post hoc] (Fig. 6A). To determine whether restoration of odorant detection translates to synaptic transmission, we examined tyrosine hydroxylase (TH) expression and glomerular morphology in the olfactory bulb (OB). OSNs project axons that extend through the cribriform plate and coalesce to form synapses with projection neurons in the glomeruli of the OB. Under normal conditions, odor-driven OSN synaptic activity induces expression of TH in postsynaptic dopaminergic juxtaglomerular interneurons (Baker et al., 1983; Baker et al., 1993; Ehrlich et al., 1990). Consistent with loss of olfactory input, we observed a twofold reduction in TH immunostaining [0.38±0.03 arbitrary units (a.u.); $F(2163)=57.11$, $P<0.0001$, one-way ANOVA, Tukey post hoc, $P<0.0001$] and decrease in glomerular size [0.44±0.01 a.u.; $F(2970)=179.8$, $P<0.0001$, one-way ANOVA, Tukey post hoc, $P<0.0001$] in *Bbs4*$^{-/-}$ mutant mice OBs (Fig. 6B–D), which are similar to other ciliopathy models (McIntyre et al., 2012; Tadenev et al., 2011; Williams et al., 2017) and attributed to axonal pathfinding defects due to loss of olfactory activity (Zheng et al., 2000; Zou et al., 2007). Analogous to the electrophysiological recordings, AV-BBS4-GFP-treated *Bbs4*$^{-/-}$ mutant mice demonstrated the return of TH immunostaining (0.64±0.05 a.u.; $P=0.0028$) and increase in glomerular size (0.68±0.02 a.u.; $P=0.0001$) (Fig. 6B–D). Together, these observations suggest that adenoviral-mediated expression of wild-type BBS4 can partially restore odor detection and postsynaptic activity within *Bbs4*$^{-/-}$ mutant mice. More importantly, a partial cilia length rescue at the cellular level was sufficient for olfactory function restoration.

DISCUSSION

Here, we provide data directly showing that global loss of BBS4 results in reduced OSN cilia length and number, as well as a decrease in ciliated HBCs without impacting the integrity of the OE. Despite the reduction in ciliation, trafficking of BBSome, IFT and olfactory signaling proteins persisted within the residual cilia of *Bbs4*$^{-/-}$ OSNs. *Bbs4*$^{-/-}$ OSN cilia also demonstrated increased IFT-B subcomplex trafficking velocities and increased IFT particle

Journal of Cell Science (2019) 132, jcs222331. doi:10.1242/jcs.222331

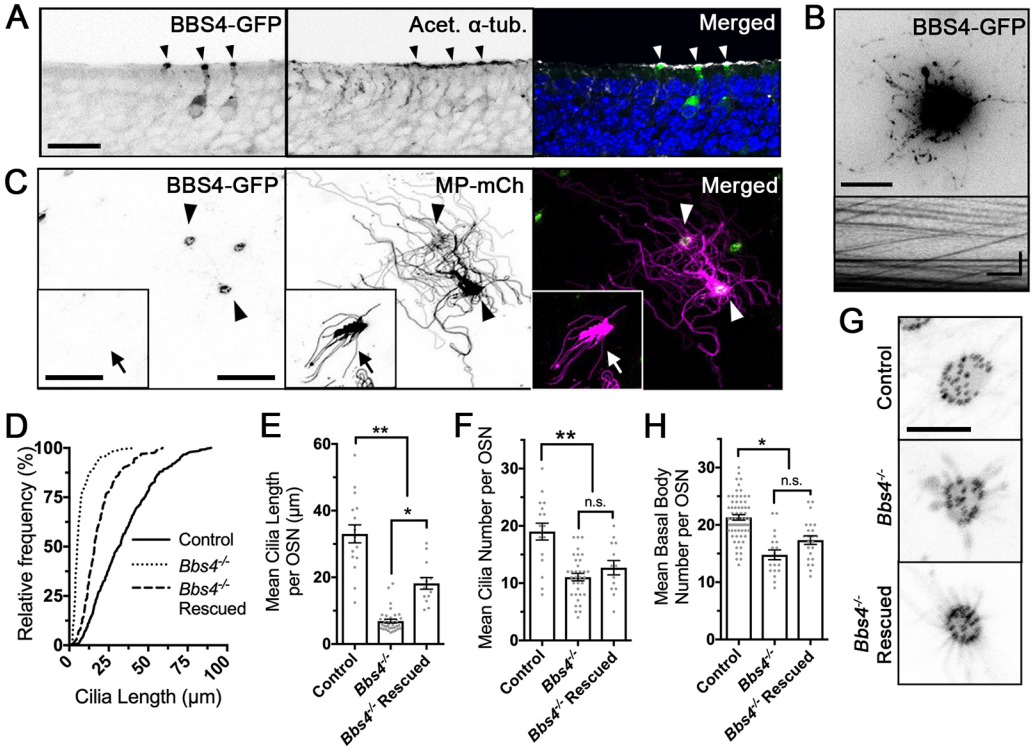

Fig. 5. Adenoviral-mediated restoration of cilia length but not cilia and basal body numbers. (A) Representative cross-section of BBS4-GFP-expressing OSNs with restoration of cilia along the apical surface. Arrowheads mark infected neurons. (B) Representative *en face* TIRFm image of BBS4-GFP-expressing *Bbs4*$^{-/-}$ OSN depicting ciliary anterograde and retrograde IFT trafficking. (C) Representative *en face* confocal image of *Bbs4*$^{-/-}$ OSNs expressing BBS4-GFP (left), MP-mCh (middle) and merged (right). *Bbs4*$^{-/-}$ OSNs infected with both BBS4-GFP and MP-mCh display restored cilia. Arrowheads mark neurons infected with BBS4-GFP + MP-mCh; arrow in inset shows neuron infected only with MP-mCh. (D) Cumulative distribution of overall cilia lengths from control (solid line), untreated *Bbs4*$^{-/-}$ (dotted line) and rescued *Bbs4*$^{-/-}$ (dashed line) OSNs measured from live *en face* confocal images. (E) Quantification of mean cilia length per OSN in control (33.0±2.7 µm per OSN; *n*=37 OSNs), untreated *Bbs4*$^{-/-}$ OSNs (6.9±0.6 µm per OSN; *n*=34 OSNs) and rescued *Bbs4*$^{-/-}$ OSNs (18.2±1.8 µm per OSN; *n*=33 OSNs) [$F(2,61)=83.95$, $P<0.0001$, one-way ANOVA, Tukey post hoc, $^{*}P<0.0001$, $^{**}P<0.0001$]. (F) Quantification of mean cilia number per OSN in control (19.0±1.5 cilia per OSN; *n*=37 OSNs), untreated *Bbs4*$^{-/-}$ OSNs (11.1±0.7 cilia per OSN; *n*=34 OSNs) and rescued *Bbs4*$^{-/-}$ OSNs (12.7±1.2 cilia per OSN; *n*=33 OSNs) [$F(2,61)=16.96$, $P<0.0001$, one-way ANOVA, Tukey post hoc, n.s., $P=0.5281$, $^{**}P<0.001$]. (G) Representative *en face* confocal images of OSN knobs expressing mCh-centrin-2 in control, *Bbs4*$^{-/-}$ and *Bbs4*$^{-/-}$ rescued OSNs expressing BBS4-GFP. (H) Quantification of mean basal body number per OSN in control (20.1±0.6 basal bodies per OSN; *n*=71 OSNs), untreated *Bbs4*$^{-/-}$ OSNs (14.8±0.8 basal bodies per OSN; *n*=19 OSNs) and rescued *Bbs4*$^{-/-}$ OSNs (17.4±0.8 basal bodies per OSN; *n*=23 OSNs) [$F(2,110)=24.61$, $P<0.0001$, one-way ANOVA, Tukey post hoc, n.s., $P=0.0933$, $^{*}P<0.0002$]. Scale bars: 20 µm (A), 10 µm (B,C,C inset), 5 µm (G), 10 s × 5 µm (kymogram in B).

frequency compared with control animals, suggesting the potential involvement of BBS4 in the coordination of IFT subcomplexes within OSN cilia (Fig. 7A). In addition, *Bbs4*$^{-/-}$ mutant mice demonstrated a reduction in OSN basal body number, which was not concomitant to cilia instability alone, underscoring a periciliary role for BBS4 in OSNs. (Fig. 7B). Together, disruption of IFT complex coupling and basal body reduction provide a model for a multimodal cause for ciliary dysfunction and disease formation in *Bbs4*$^{-/-}$ mutant mice. Furthermore, assessment of adenoviral gene replacement shows that AV-BBS4-GFP-infected mature OSNs exhibited increased ciliary lengths but ciliary and basal body numbers were not restored. Despite the partial ciliary restoration, odorant detection at the periphery and synaptic-dependent activity within the OB were rescued in AV-BBS4-GFP-treated *Bbs4*$^{-/-}$ mutant mice.

BBS4 loss disrupts ciliary protein trafficking, but not entry

Analysis of OSN cilia in BBS mutants uncovered novel phenotypes associated with the loss of specific BBSome subunits in mammalian cells. It is known through hierarchal analysis of BBSome complex assembly that BBS1 and BBS4 are in close association. Specifically, the incorporation of BBS4 into the BBSome complex depends on BBS1 (Zhang et al., 2012). This finding is supported by observations in *Chlamydomonas reinhardtii*, in which disruption of BBS1 affects BBS4 stability or expression (Lechtreck et al., 2009). In addition, recent data suggest that the BBSome associates with IFT particles prior to ciliary entry, with BBS1 as a central protein linking the BBSome and IFT complexes (Wei et al., 2012). This is consistent within OSN cilia, where previous work showed that BBS1 loss resulted in a failure of BBSome protein entry into the cilia, despite the persistence of IFT particle movement (Williams et al., 2017). On the other hand, as shown here, loss of BBS4 did not impede ciliary localization of BBSome proteins into residual *Bbs4*$^{-/-}$ OSN cilia. This is in contrast to previous *in vitro* studies, which indicated that all BBSome components are required for BBSome ciliary entry (Seo et al., 2011).

Although BBS4 loss did not alter BBSome entry into cilia, it did affect IFT particle movement within the OSN cilia of mutant animals. The selective increase of IFT-B particle trafficking velocity in *Bbs4*$^{-/-}$ OSN cilia is in agreement with *Caenorhabditis elegans*, in which loss of the BBS proteins resulted in increased IFT-B trafficking velocities in the sensory cilia (Ou et al., 2005). Our observations, measured for the first time within the intact mammalian cilium of a genetic model, showed the miscoordination of the two IFT subcomplexes, which adds to the hypothesis that the BBSome

Journal of Cell Science (2019) 132, jcs222331. doi:10.1242/jcs.222331

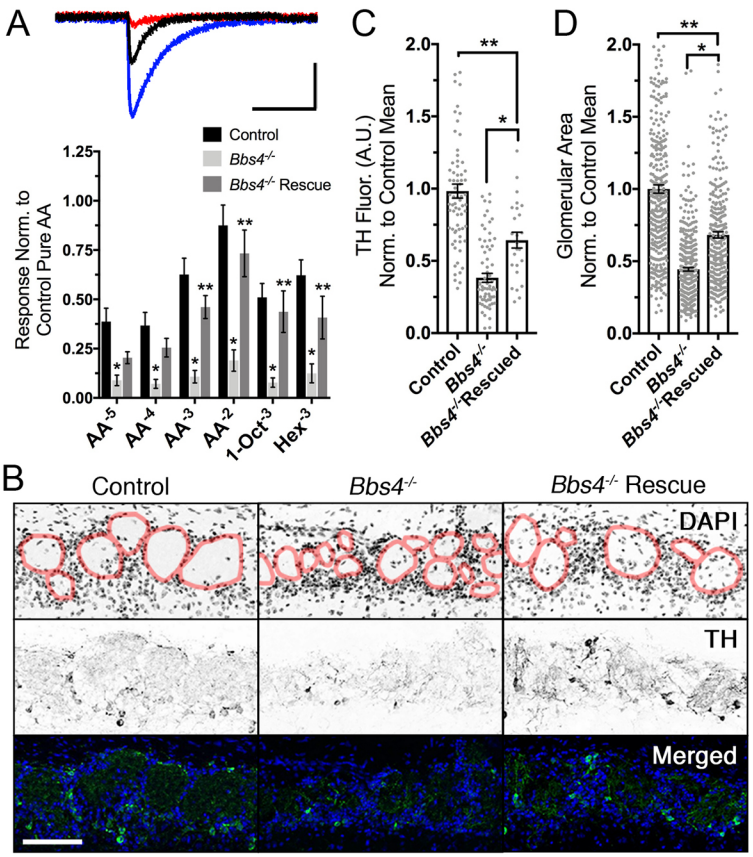

Fig. 6. Adenoviral-mediated restoration of olfactory detection and synaptic activity. (A) (Top) Representative electro-olfactogram (EOG) traces from control (blue), *Bbs4*$^{-/-}$ (red) and *Bbs4*$^{-/-}$ rescue (black) mice in response to 10^{-3} M amyl-acetate (AA). (Bottom) Mean odorant-mediated EOG responses to 10^{-3} M AA, 10^{-3} M 1-octanol (1-Oct) and 10^{-3} M hexanal (Hex). EOG responses were decreased in untreated *Bbs4*$^{-/-}$ mice (n=14 animals) compared with controls (n=18 animals), and increased in *Bbs4*$^{-/-}$ rescued (n=11 animals) compared with untreated *Bbs4*$^{-/-}$ mice [F(2346)=52.11, P<0.0001, two-way ANOVA, Tukey post hoc, *P<0.01, **P<0.02]. (B) Restoration of tyrosine hydroxylase (TH) immunostaining and glomerular size, as demarcated by the red borders, in *Bbs4*$^{-/-}$ mice treated with AV-BBS4-GFP. (C) Quantification of normalized TH intensity in control (0.98±0.05 a.u.; n=7 animals), *Bbs4*$^{-/-}$ (0.38±0.03 a.u.; n=8 animals), *Bbs4*$^{-/-}$ rescued mice (0.64±0.05 a.u.; n=7 animals) [F(2163)=57.11, P<0.0001, one-way ANOVA, Tukey post hoc, *P<0.0001, **P=0.0028]. (D) Quantification of normalized glomerular area in control (1.0±0.03 a.u.; n=7 animals), *Bbs4*$^{-/-}$ (0.44±0.01 a.u.; n=8 animals), *Bbs4*$^{-/-}$ rescued mice (0.68±0.02 a.u.; n=7 animals) [F(2970)=179.8, P<0.0001, one-way ANOVA, Tukey post hoc, *P<0.0001, **P=0.0001]. Scale bars: 10 s×5 mV (A), 10 µm (B).

and its individual proteins are necessary for the proper assembly of the IFT complex (Blacque et al., 2004; Ou et al., 2005; Snow et al., 2004; Xu et al., 2015). It also supports the idea that the BBSome is a cargo adapter rather than a component of the IFT machinery (Lechtreck, 2015; Lechtreck et al., 2009). Comparison of IFT subcomplex movement between *Bbs1* KO and *Bbs4*$^{-/-}$ OSN cilia alludes to a model in which the BBSome is IFT cargo with BBS4 coordinating IFT-A and IFT-B movement (Fig. 7A). Our results, based on differential IFT subcomplex velocities combined with the continual entry of BBSome proteins in the OSN cilia, suggest that, in the absence of BBS4, the BBSome cargo may remain tethered to the IFT-A but not the IFT-B particle. This is consistent with studies in invertebrate models, in which the BBSome was shown to be required for IFT particle assembly and the trafficking of cargo to and from the cilia (Lechtreck, 2015; Wei et al., 2012).

In addition to particle velocities, we also observed increases in anterograde and retrograde IFT particle frequencies in the residual *Bbs4*$^{-/-}$ OSN cilia. The inverse relationship between cilia length and particle frequency had been previously observed within *C. reinhardtii*, where shorter regenerating cilia exhibited increased anterograde IFT trafficking frequencies (Craft et al., 2015; Engel et al., 2009; Wren et al., 2013). The increase in frequency is hypothesized to enhance transportation and delivery of ciliary components to the tip in order to accommodate ciliary growth. As BBS4 loss does not result in the complete abolishment of cilia and retain IFT/BBSome trafficking, it is plausible that the alteration in the dynamics is a consequence of active ciliary assembly and growth. However, owing to the absence of BBS4, and presumably reduction in BBSome function, this may result in an imbalance of ciliary maintenance favoring ciliary disassembly over assembly. Alternatively, the increased IFT particle frequency may be attributed to a BBS4-dependent regulation of particle size. Despite appearing as distinct puncta under TIRFm, IFT particles are more accurately represented as macromolecular trains. Under detailed electron tomography, the individual IFT trains are assembled as multiprotein arrays consisting of several IFT complexes, motor proteins and cargo proteins (Pigino et al., 2009; Stepanek and Pigino, 2016; Vannuccini et al., 2016). More importantly, these trains are highly dynamic structures and routinely undergo substantial reorganization at the ciliary tip (Chien et al., 2017). The absence of BBS4, or the BBSome, may impact macromolecular assembly or composition of the IFT train. Although the *C. reinhardtii* flagella exhibit substoichiometric amounts of BBSome incorporated into the IFT train (Brown et al., 2015; Lechtreck et al., 2009), the 1:1 stoichiometric relationship found within OSN cilia (Williams et al., 2014) might suggest a more prominent role of BBSome proteins in train assembly. Therefore, the absence of a functional BBSome may result in an improperly assembled IFT train, which, in turn, could lead to altered particle frequency and trafficking rates. Although IFT trains have been observed in mammalian cilia (Lechtreck, 2015), details regarding the presence of IFT trains within OSN cilia and the role of the BBSome in their assembly will require detailed molecular studies and further investigation.

Besides the entry and trafficking dynamics of ciliary proteins, *Bbs4*$^{-/-}$ mutant OSNs retained ciliary trafficking of both endogenous and ectopically expressed olfactory signaling proteins. This indicates that *Bbs4*$^{-/-}$ mutant OSNs maintain the ability to transduce odor-mediated responses, and the loss of olfactory function is likely attributed to the loss of ciliary structure, as supported by past conclusions (Kulaga et al., 2004). Secondly, BBS4 loss does not prevent transmembrane protein entry into OSN cilia. This observation is contrary to *in vitro* and *in vivo* studies that have implicated the BBSome in the ciliary entry of proteins (Berbari et al., 2008; Jin et al., 2010; Loktev and Jackson, 2013). Specifically, the absence of BBS4

Journal of Cell Science (2019) 132, jcs222331. doi:10.1242/jcs.222331

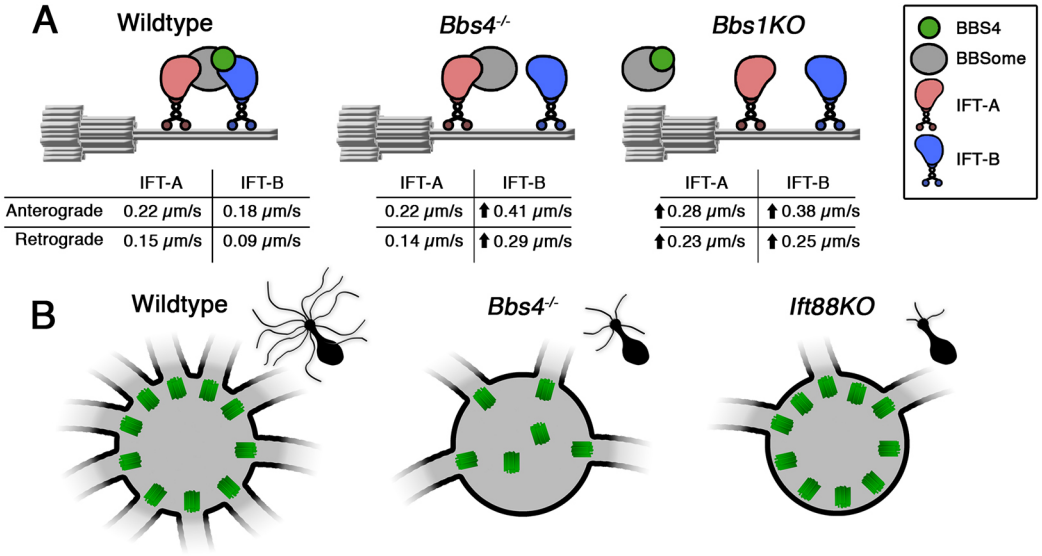

Fig. 7. Summary diagram for mechanism of cilia loss in *Bbs4*$^{-/-}$ mutant mice. (A) Diagram depicting the IFT subcomplex decoupling in the absence of BBS4 and BBS1 within the OSN cilia. (Left) Under normal conditions, the BBSome complex (gray) functions as a bridge connecting the IFT-A (red) and IFT-B (blue) subcomplexes and their respective motors. (Right) In the absence of BBS1, the BBSome fails to enter the cilia, while the IFT subcomplexes retain ciliary trafficking. With the loss of BBSome cilia entry, the IFT-A and IFT-B subcomplexes are miscoordinated and both exhibit faster trafficking velocities compared with wild-type controls. (Middle) In the absence of BBS4 (green), the BBSome and IFT subcomplexes retain cilia entry and trafficking. However, the IFT-B subcomplex is decoupled from the IFT-A subcomplex, with IFT-B exhibiting increased trafficking velocities, while IFT-A velocities remain unchanged. (B) Diagram depicting basal body disruption in *Bbs4*$^{-/-}$ and *Ift88* KO OSN knobs with respective cilia morphologies (top-right insets). (Left) Under wild-type conditions, individual basal bodies (green) associate with OSN cilia. (Middle) In the absence of BBS4, basal body numbers are reduced, with some failing to associate with cilia. (Right) Despite significant ciliary loss, the absence of IFT88 did not alter basal body numbers. This suggests that the basal body-mediated reduction is specific to BBS4 and not ciliary loss.

resulted in relatively normal primary ciliation, but induced ciliary mislocalization of somatostatin receptor 3 (SSTR3) and melanin-concentrating hormone receptor 1 (MCHR1) in hippocampal tissues (Berbari et al., 2008), and TrkB (also known as NTRK2) receptor in BDNF activation in cell cultures (Leitch and Zaghloul, 2014). However, other studies have suggested the role of the BBSome in the extraciliary trafficking and export of receptors (Domire et al., 2011; Eguether et al., 2014; Liew et al., 2014; Nager et al., 2017; Ye et al., 2018), channels (Xu et al., 2015), phospholipases (Liu and Lechtreck, 2018) and other membrane-bound proteins (Lechtreck et al., 2009; Lechtreck et al., 2013). Activated GPCRs facilitate BBSome and IFT enrichment at the tip of cilia for eventual retrieval and export (Ye et al., 2018). Disruption of this mechanism, as in BBS4 depletion, resulted in the accumulation of the activated GPCRs at the ciliary tip, leading to swelling and excision of the tip as mechanism for regulating ciliary content (Nager et al., 2017). Although this process has yet to be directly observed *in vivo*, and the activation state of the observed odorant receptors is unknown, structural studies from *Bbs1*-null (Carter et al., 2012) and *Bbs2-*, *Bbs4-* and *Bbs6*-null (Shah et al., 2008) cells, including our own *en face* imaging of some *Bbs4*$^{-/-}$ mutant OSNs, revealed the formation of swellings at the ciliary tip, hinting at a possible shedding mechanism. Despite the unperturbed ciliary entry of odorant receptors and signaling proteins in *Bbs4*$^{-/-}$ mutant OSNs, we also cannot exclude disruption to transmembrane protein steady-state entry/exit dynamics. Therefore, additional experimentation is necessary to elucidate these mechanisms within normal and ciliopathy OSN cilia.

A role for BBS4 in stability of OSN cilia and basal bodies

Basal body and cilia biogenesis occurs through a tightly regulated process of centriole duplication, axonemal extension, and protein and vesicle recruitment to the plasma membrane (Pearson and Winey, 2009; Sánchez and Dynlacht, 2016). According to transmission electron microscopy studies, mammalian OSN basal body formation begins with centriole duplication near the perinuclear region at embryonic day (E) 11, when the apical dendrite begins to form and extend toward the surface (Cuschieri and Bannister, 1975; Jenkins et al., 2009; Menco, 1980; Menco and Farbman, 1985). When the dendritic knob is fully formed by E12, the basal bodies mature when the centrioles are anchored to the plasma membrane, which is then followed by axonemal extension. Beyond these structural studies, little is understood about basal body biogenesis and maintenance within mature OSNs. Using live *en face* imaging, we were able to resolve individual basal bodies and show incorporation of ectopically expressed tagged γ-tubulin and centrin-2 into the basal bodies of mature OSNs. This observation suggests that basal bodies are dynamic structures and exhibit continual protein incorporation after nascent ciliogenesis, a process that was first documented in *T. thermophila* (Pearson et al., 2009). In regards to basal body number, its reduction in the dendritic knobs of *Bbs4*$^{-/-}$ OSNs highlights a potential role of BBS4 in basal body maintenance. BBSome proteins were shown to associate with the basal body and were largely understood to facilitate trafficking of signaling molecules in addition to other proteins to the cilia (Berbari et al., 2008; Seo et al., 2009). BBS4, in particular, was demonstrated to interact with several pericentriolar proteins such as dynactin subunit 1, a protein that interacts with microtubules and dynein, and pericentriolar material 1 protein (PCM-1), a core protein in the centriolar satellites that was also mislocalized in *Bbs4*$^{-/-}$ mutant hair cells (Chamling et al., 2014; Kim et al., 2004; May-Simera et al., 2009; Wang et al., 2016). Interestingly, although loss of PCM-1 indicates defects in ciliogenesis (Wang et al., 2016), disruption of other basal body-associated proteins phenotypically mimics *Bbs4*$^{-/-}$ mutant OE. Specifically, deletion of centrin-2

Journal of Cell Science (2019) 132, jcs222331. doi:10.1242/jcs.222331

(Ying et al., 2014) and hypomorphic mutations of pericentrin (Miyoshi et al., 2009) resulted in OSN cilia loss without affecting respiratory cells. More importantly, although basal body formation and stability are critical for ciliogenesis, cilia loss does not necessarily lead to basal body degradation. This was evident by the unaltered basal body numbers in the olfactory-specific *Ift88* KO mouse model in this study, and the normal basal body organization in IFT88-depleted *Paramecium tetraurelia* (Picariello et al., 2014). These observations support the idea that basal body reduction is not concomitant to cilia loss. However, because cilia and basal bodies appeared structurally intact in hippocampal and amygdala neurons, as well as multiciliated cells in *Bbs4*$^{-/-}$ mutant mice (Agassandian et al., 2014; Shah et al., 2008; Swiderski et al., 2012), the impact of BBS4 loss on OSNs basal bodies could be unique to these neurons. It is possible that OSNs utilize alternative mechanisms for basal body biogenesis and maintenance that makes the neurons sensitive to loss in the absence of BBS4.

Differential penetrance and therapeutic implications

As summarized in a recent review (Reiter and Leroux, 2017), not all ciliopathies demonstrate the same degree of penetrance across the body or within tissues. This complexity is highlighted by the fact that cilia are not lost in all tissues of *Bbs4*-null animals. Cilia persist in the amygdala and hippocampus within the brain and in the renal cells of the kidney in *Bbs4*$^{-/-}$ mutant mice (Agassandian et al., 2014; Berbari et al., 2008; Mokrzan et al., 2007; Mykytyn et al., 2004). Within the nasal cavity, respiratory cells were not affected by the loss of BBS4, corroborating prior structural and functional studies (Kulaga et al., 2004; Shah et al., 2008). Within the OE, *Bbs4*$^{-/-}$ mutant mice showed a reduction in cilia from OSNs as well as primary ciliated HBCs. This suggests that differential penetrance of BBS4 deletion is not simply due to primary versus multiciliation. Although loss of HBC ciliation did not influence the establishment of the OE, this study underscores involvement of HBC cilia signaling in the recovery of the OE following chemical lesion (Joiner et al., 2015). The reduction in the ability for *Bbs4*$^{-/-}$ mutant OE to recover after lesion might imply the susceptibility of BBS4 patients to incur added olfactory loss following injury. In addition, the integrity of *Bbs4*$^{-/-}$ mutant OE may be impacted at older timepoints, when neurogenic exhaustion and accelerated neuronal turnover are prominent (Schwob et al., 2017). At our observed ages (P20–35), the integrity of the OE of *Bbs4*$^{-/-}$ mutant mice was retained, similar to other ciliopathy mouse models (Green et al., 2018; Tadenev et al., 2011; Williams et al., 2017). This stability makes the olfactory system distinct from other sensory systems such as the retina, where cilia loss leads to neurodegeneration (Mykytyn et al., 2004).

Mechanistically, we demonstrated a bimodal impact of BBS4 loss on the cilia and basal bodies of OSNs. It possible that other ciliopathies may follow a similar mechanism, accounting for the penetrance in certain tissue types. Different cell types may vary in their ability to tolerate the disruptions in protein trafficking and basal body maintenance and/or stability, resulting in differential phenotypes. Therapeutically, the partial restoration of the ciliary lengths in AV-BBS4-GFP-infected OSNs was sufficient to restore olfactory detection and synaptic activity. However, it remains unclear whether restoration of cilia length alone is sufficient to restore course and fine behaviors in treated *Bbs4*$^{-/-}$ mutant mice. If restoring the full complement of OSN cilia is necessary, then the therapeutic strategy may be shifted earlier in development during nascent basal body and/or ciliogenesis to ensure stability, promote formation and prevent degradation. Transgenic expression of BBS4 into *Bbs4*-null mice was able to complement the deficiency of BBS4 early in development and rescue all of the BBS phenotypes (Chamling et al., 2013). Therefore, early intervention involving embryonic, perinatal or early postnatal treatment may improve the efficacy of the therapy by targeting developing or immature OSNs prior to ciliogenesis and basal body formation. Alternatively, directly targeting the olfactory basal stem cells in adults could be therapeutically advantageous, as the current method of intranasal gene delivery excludes the deeper cell populations. Nonetheless, our positive results in the olfactory system further add to the growing capacity of gene replacement therapy to target and treat BBS-related dysfunctions, as well as other congenital diseases afflicting the peripheral olfactory system.

MATERIALS AND METHODS

Mice

All procedures were approved by the University of Florida Institutional Animal Care and Use Committee. Unless indicated, mice of both sexes (P20–35) were utilized for all experimentation and were housed in a standard animal facility room at the University of Florida. Global *Bbs4* knockout (*Bbs4*$^{-/-}$) mice were provided by V. C. Sheffield (Mykytyn et al., 2004). *Bbs4* knockout alleles were maintained on B6/126sv background. OSN conditional deletion of *Ift88* (*Ift88* KO) (Green et al., 2018) was achieved previously by crossing mice with the heterozygous *OMP-Cre* allele (Li et al., 2004) with those containing a floxed *Ift88*$^{fl/\Delta}$ allele (Haycraft et al., 2007). OSN conditional deletion of *Bbs1* (*Bbs1* KO) was achieved previously by crossing mice with the heterozygous *OMP-Cre* allele with those containing floxed *Bbs1*$^{fl/fl}$ (Carter et al., 2012; Williams et al., 2017). For DNA extraction, tail clippings were digested with 75 µl alkaline lysis reagent (25 mM NaOH, 0.2 mM Na_2-EDTA $2H_2O$, pH 12.0) in a 95-degree shaker for 20 min, followed by the addition of 75 µl neutralization reagent (40 mM Tris-HCl, pH 5.0) at room temperature (Wang and Storm, 2006). For genotyping, 2.0 µl of samples was mixed with 0.9 µl primer cocktail mix, 4.6 µl H_2O and 7.5 µl GoTaq Green Mastermix (Promega), with the mixture run through the genotyping cycle available at the Jackson Laboratory (stock 010728).

Immunohistochemistry

Mice were deeply anesthetized with an intraperitoneal injection of xylazine (100 mg/kg) and ketamine (10 mg/kg), transcardially perfused with 4% paraformaldehyde (PFA) in 1× PBS and snouts were dissected. Isolated snouts were then incubated in 4% PFA overnight at 4°C, decalcified in 0.5 M EDTA/1× PBS for 48 h, then were cryoprotected in 10%, 20% and 30% sucrose in 1× PBS for 1 h, 1 h and overnight, respectively, at 4°C, and embedded in OCT compound (TissueTek). Embedded tissues were cryosectioned along the coronal plane at a thickness of 12 µm on a Leica CM1860 cryostat and mounted onto Superfrost Plus slides (Fisher Scientific). For immunostaining, cryosections were permeabilized and blocked with 0.1% Triton X-100 and 2% donkey serum in 1× PBS for 30 min. Primary antibodies were diluted in 2% donkey serum and applied to samples for 1 h at room temperature. When multiple primary antibodies were used, incubations with each antibody were performed sequentially, and samples were washed three times with 1× PBS between each incubation. Primary antibodies were used at the following concentrations: mouse anti-acetylated α-tubulin (1:1000, clone 6-11 B-1, T6793, Sigma-Aldrich); goat anti-OMP (1:1000, 544-10001, Wako); rabbit anti-adenylyl cyclase III (ACIII; 1:1000, RPCA-ACIII, EnCor Biotechnology); rabbit anti-CNGA2 (1:1000, APC-045, Alomone Labs); mouse anti-mOR28 (1:500, OSR00212W, Thermo Fisher Scientific); rabbit anti-TH (1:500, MAB318, Millipore). Fluorescent-conjugated secondary antibodies were applied (at 1:1000 dilution) for 1 h, and sections were then washed three times with PBS. Then, 4′,6-diamidino-2-phenylindole (DAPI) was applied for 5 min to stain nuclei, and samples were mounted using Prolong Gold (Invitrogen). Fixed tissue imaging was performed on a Nikon TiE-PFS-A1R confocal microscope equipped with a 488 nm laser diode with a 510–560 nm band pass filter, 561 nm laser with a 575–625 nm band pass filter

Journal of Cell Science (2019) 132, jcs222331. doi:10.1242/jcs.222331

and a 640-nm laser with a 663–738 nm band pass filter, using CFI Apochromat Lambda 10× 0.45 NA, 20× 0.75 NA and 60× 1.4 NA objectives. Confocal *Z*-stacks were processed using NIH ImageJ software.

Whole-mount *en bloc* immunohistochemistry

Freshly dissected turbinates and septum from mouse snouts were drop fixed for 3–4 h on ice in freshly prepared 4% PFA in 1× PBS (pH7.4) supplemented with 20% sucrose. Tubes containing the tissue were carefully placed in a refrigerator and left for the duration of fixation without agitation to limit mechanical damage to the cilia. The tissue was thoroughly washed in 1× PBS, then blocked with PBS containing 3% fetal bovine serum, 2% bovine serum albumin and 0.3% Triton X-100 for 2 h at room temperature. The tissue was then incubated with primary antibody against mouse M71/72 olfactory receptor (gift from Dr Gilad Barnea, Brown University, Providence, RI) raised in guinea pig, diluted 1:1000 in the same blocking solution. Finally, the tissue was incubated with secondary anti-guinea pig Alexa Fluor 568 (1:1000) for 2 h and placed in antifading mounting agent Vectashield (Vector Labs) on the glass coverslip.

OE ablation

Two- to three-month-old wild-type control and *Bbs4*$^{-/-}$ mutant mice from both sexes received a single intraperitoneal injection of methimazole (MMZ; 2-mercapto-1-methylimidazole; M8506, Sigma-Aldrich) (75 mg/kg in sterilized 1× PBS). Following treatment, mice were allowed to recover for 8 weeks after chemical ablation as previously outlined (Bergman and Brittebo, 1999; Joiner et al., 2015). At 8 weeks post-treatment, mice were euthanized, and tissue was collected, processed and immunostained as described above.

SEM

Mice were placed under deep anesthesia and subjected to cardiac perfusion with 2% glutaraldehyde and 0.15 M cacodylate in water. Olfactory turbinates were dissected and processed using the OTOTO protocol. Analysis was performed on an Amray (Drogheda) 1910FE field emission scanning electron microscope at 5 kV and recorded digitally with Semicaps software (SEMICAPS PTE Ltd, Singapore).

Vectors

Plasmids containing mouse cDNA fragments were provided as follows: ACIII (R. Reed, Johns Hopkins University, Baltimore, MD); CNGB1 (R. L. Brown, Oregon Health and Science University, Portland, OR); M71 (#15635, Addgene); BBS4, BBS2, BBS3 and BBS5 (K. Mykytyn, Ohio State University, Columbus, OH); IFT88 (B. K. Yoder, The University of Alabama at Birmingham, Birmingham, AL); IFT122 (J. Eggenschwiler, University of Georgia); centrin-2 (#41147, Addgene); γ-tubulin (#55050, Addgene). Myristoylated-palmitoylated-GFP/mCherry (MyrPlam-GFP-mCh) was described previously (Williams et al., 2014; Williams et al., 2017; Zacharias et al., 2002). All cDNAs were fused with GFP or mCherry and inserted into the pAd/CMV/V5-DEST™ expression vector using Gateway® technology (Invitrogen). Adenoviral vectors were propagated using the ViraPower protocol (Invitrogen), isolated with the Virapur Adenovirus mini purification Virakit (Virapur, San Diego, CA) and dialyzed in 2.5% glycerol, 25 mM NaCl and 20 mM Tris-HCl, pH 8.0 (Slide-A-Lyzer Dialysis Cassette, 66383, Thermo Fisher Scientific) overnight. All generated adenoviral vectors yielded ∼10×10^9 plaque-forming units. Samples were aliquoted and stored at −80°C, until use.

Ectopic gene delivery

Adenoviral doses (20 µl) were administered directly to the nasal cavity of mice on three consecutive days. Mice beyond wean age (P21) were lightly anesthetized with isoflurane prior to each adenoviral treatment. For all animals, experiments were performed 10 days following the final administration of adenovirus to allow for sufficient protein expression. All intranasal deliveries used a pulled 1-ml syringe and trimmed to 0.5 mm tip (309659, Becton Dickinson) (McIntyre et al., 2012; Williams et al., 2014; Williams et al., 2017). All mice were positioned vertically and adenoviral solutions were delivered as 1.0 mm diameter droplets (equivalent to 3–4 µl) in alternating nostrils, while avoiding the philtrum. Quantification of adenoviral infection rates was performed by counting the number of GFP-positive cells per millimeter OE from both coronal and *en face* samples of *Bbs4*$^{-/-}$ mutant mice.

Live *en face* confocal imaging

For live *en face* confocal imaging, virally transduced animals were euthanized with CO_2, rapidly decapitated and split along the cranial midline. Olfactory turbinates were exposed by removing the nasal bone and any remaining septal tissue. For each intact hemisected snout, tissue rostral to the turbinates and 1 mm caudal of the olfactory bulb were removed. With the medial surface down on the coverslip, the tissue was placed into the imaging chamber containing artificial cerebrospinal fluid (124 mM NaCl, 3 mM KCL, 1 mM $MgCl_2$, 2 mM $CaCl_2$, 1.25 mM NaH_2PO_4, 26 mM $NaHCO_3$, 25 mM glucose) bubbled with 5% CO_2/95% O_2 for >10 min prior to use. For proper imaging, tissues were held down using a mesh within the imaging chamber. The assembled imaging chamber was subsequently placed in a secondary tissue chamber and imaged on a Nikon TiE-PFS-A1R confocal microscope (described above). Cilia length measurements, and cilia and basal body number counts were performed using ImageJ on a Wacom touch display (DTF-720). Data from all mice are presented as mean±s.e.m., with the unpaired *t*-test used for characterization experiments and ANOVA with Tukey's post hoc pairwise comparisons used for the rescue experiments.

Live *en face* TIRFm imaging

For *en face* TIRFm imaging, virally transduced animals were prepared as above. TIRFm time series were captured at 200 ms exposure with zero delay interval for 2–3 min on a Nikon Eclipse Ti-E/B inverted microscope equipped with a 100× CFI APO TIRF 1.49 NA, 1.5× tube lens, ZT488/561rpc dichroic, ZET488/561x excitation filter, ZET488/561m TRF emission filter (Chroma Technology) and an EMCCD camera (iXon X3 DU897, Andor Technology). The 488-nm line of a fiber-coupled diode laser at incident power of 2 mW was used to illuminate a circular region of ∼60 µm in diameter for capturing video sequences at 5–10 Hz. ImageJ was used to generate line-scan kymograms for measuring particle velocities and counts from imported time series. Particle velocities were calculated as such [velocity=tan(θ)], where θ is the angle of deflection form the horizontal on a kymogram with time (s) and distance (µm) on the *x*-axis and *y*-axis, respectively. Particle counts were determined based on number of moving particles, as determined by kymogram, per duration of recording. Data from all mice are presented as mean±s.e.m., with the unpaired *t*-test used for BBS5 and particle frequencies, and ANOVA with Tukey's post hoc pairwise comparisons used for trafficking velocities.

EOG

Mice were killed with CO_2, rapidly decapitated and split along the cranial midline. Septal tissue was removed to expose olfactory turbinates and the intact hemisected preparation was mounted in a Sylgard-lined chamber. Vapor-phase odor stimuli were generated as follows: a 1 M odorant stock solution was diluted 1:10 (in dimethyl sulfoxide) and then mixed to the final (reported) dilution in ultrapure water. Single molecule odorants used were AA (W504009, Sigma-Aldrich), 1-Oct (O4500, Sigma-Aldrich) and Hex (115606, Sigma-Aldrich). Odorants were delivered via a picospritzer controlled by pCLAMP software (version 9.2, Molecular Devices) as a 100-ms pressurized pulse injected into a continuous stream of humidified air flowing over the tissue. Electrodes (1–3 mOhm) were made of borosilicate glass capillaries filled with 0.5% SeaPlaque agarose (Lonza) in modified Ringer's solution (135 mM NaCl, 5 mM KCl, 1 mM $CaCl_2$, 1.5 mM $MgCl_2$ and 10 mM HEPES, pH 7.4). Responses to odor stimuli were recorded from turbinates IIa and IIb using a Multiclamp 700A amplifier controlled by pClamp software (version 9.2, Molecular Devices). EOG responses were measured as the maximal peak amplitude from the pre-pulse baseline using Clampfit software (Molecular Devices). Data were normalized to the mean response to pure AA in wild-type littermate control mice and presented as mean±s.e.m. Statistical analyses comparing wild-type littermate control, *Bbs4*$^{-/-}$ and *Bbs4*$^{-/-}$ rescued mice were performed using two-way ANOVA with Tukey's post hoc pairwise comparisons.

Acknowledgements
We acknowledge L. Bayer (University of Michigan) and the University of Michigan Microscopy and Image Analysis Laboratory for assistance with SEM. Intellectual support was provided by members of the University of Florida Center for Smell and Taste.

Competing interests
The authors declare no competing or financial interests.

Author contributions
Conceptualization: C.R.U., C.L.W., J.R.M.; Methodology: C.R.U., C.L.W.; Formal analysis: C.R.U., C.L.W., C.X., D.T.S., W.W.G., K.U.; Investigation: C.R.U., C.L.W., C.X., D.T.S., W.W.G., K.U.; Resources: C.R.U., L.Z., D.Y.N., V.C.S.; Data curation: C.R.U.; Writing - original draft: C.R.U., J.R.M.; Writing - review & editing: C.R.U., J.R.M., V.C.S.; Visualization: C.R.U., J.R.M.; Supervision: J.R.M.; Project administration: J.R.M.; Funding acquisition: V.C.S., J.R.M.

Funding
This work was supported by the National Institute on Deafness and Other Communication Disorders [R01 DC009606 to J.R.M.] and the National Eye Institute [R01 EY017168 to V.C.S.]. Deposited in PMC for release after 12 months.

Supplementary information
Supplementary information available online at
http://jcs.biologists.org/lookup/doi/10.1242/jcs.222331.supplemental

References

Abd-El-Barr, M. M., Sykoudis, K., Andrabi, S., Eichers, E. R., Pennesi, M. E., Tan, P. L., Wilson, J. H., Katsanis, N., Lupski, J. R. and Wu, S. M. (2007). Impaired photoreceptor protein transport and synaptic transmission in a mouse model of Bardet–Biedl syndrome. *Vision Res.* **47**, 3394-3407.

Agassandian, K., Patel, M., Agassandian, M., Steren, K. E., Rahmouni, K., Sheffield, V. C. and Card, J. P. (2014). Ciliopathy is differentially distributed in the brain of a Bardet-Biedl syndrome mouse model. *PLoS One* **9**, e93484.

Aldahmesh, M. A., Li, Y., Alhashem, A., Anazi, S., Alkuraya, H., Hashem, M., Awaji, A. A., Sogaty, S., Alkharashi, A., Alzahrani, S. et al. (2014). IFT27, encoding a small GTPase component of IFT particles, is mutated in a consanguineous family with bardet-biedl syndrome. *Hum. Mol. Genet.* **23**, 3307-3315.

Baker, H., Kawano, T., Margolis, F. L. and Joh, T. H. (1983). Transneuronal regulation of tyrosine hydroxylase expression in olfactory bulb of mouse and rat. *J. Neurosci.* **3**, 69-78.

Baker, H., Morel, K., Stone, D. M. and Maruniak, J. A. (1993). Adult naris closure profoundly reduces tyrosine hydroxylase expression in mouse olfactory bulb. *Brain Res..* **614**, 109-116.

Bayless, B. A., Galati, D. F., Junker, A. D., Backer, C. B., Gaertig, J. and Pearson, C. G. (2016). Asymmetrically localized proteins stabilize basal bodies against ciliary beating forces. *J. Cell Biol.* **215**, 457-466.

Berbari, N. F., Lewis, J. S., Bishop, G. A., Askwith, C. C. and Mykytyn, K. (2008). Bardet-Biedl syndrome proteins are required for the localization of G protein-coupled receptors to primary cilia. *Proc. Natl. Acad. Sci. USA* **105**, 4242-4246.

Bergman, U. and Brittebo, E. B. (1999). Methimazole toxicity in rodents: covalent binding in the olfactory mucosa and detection of glial fibrillary acidic protein in the olfactory bulb. *Toxicol. Appl. Pharmacol* **155**, 190-200.

Billingsley, G., Deveault, C. and Héon, E. (2011). BBS mutational analysis: a strategic approach. *Ophthalmic Genet.* **32**, 181-187.

Blacque, O. E., Reardon, M. J., Li, C., McCarthy, J., Mahjoub, M. R., Ansley, S. J., Badano, J. L., Mah, A. K., Beales, P. L., Davidson, W. S. et al. (2004). Loss of C. elegans BBS-7 and BBS-8 protein function results in cilia defects and compromised intraflagellar transport. *Genes Dev.* **18**, 1630-1642.

Brown, J. M., Cochran, D. A., Craige, B., Kubo, T. and Witman, G. B. (2015). Assembly of IFT trains at the ciliary base depends on IFT74. *Curr. Biol.* **25**, 1583-1593.

Burton, P. R. (1992). Ultrastructural studies of microtubules and microtubule organizing centers of the vertebrate olfactory neuron. *Microsc. Res. Tech.* **23**, 142-156.

Burton, P. R. and Laveri, L. A. (1985). The distribution, relationships to other organelles, and calcium-sequestering ability of smooth endoplasmic reticulum in frog olfactory axons. *J. Neurosci.* **5**, 3047-3060.

Carter, C. S., Vogel, T. W., Zhang, Q., Seo, S., Swiderski, R. E., Moninger, T. O., Cassell, M. D., Thedens, D. R., Keppler-Noreuil, K. M., Nopoulos, P. et al. (2012). Abnormal development of NG2+PDGFR-α+ neural progenitor cells leads to neonatal hydrocephalus in a ciliopathy mouse model. *Nat. Med.* **18**, 1797-1804.

Chamling, X., Seo, S., Bugge, K., Searby, C., Guo, D. F., Drack, A. V., Rahmouni, K. and Sheffield, V. C. (2013). Ectopic expression of human BBS4 can rescue bardet-biedl syndrome phenotypes in Bbs4 null mice. *PLoS One* **8**, e59101.

Chamling, X., Seo, S., Searby, C. C., Kim, G., Slusarski, D. C. and Sheffield, V. C. (2014). The centriolar satellite protein AZI1 interacts with bbs4 and regulates ciliary trafficking of the BBSome. *PLoS Genet.*. **10**, e1004083.

Chien, A., Shih, S. M., Bower, R., Tritschler, D., Porter, M. E. and Yildiz, A. (2017). Dynamics of the IFT machinery at the ciliary tip. *Elife* **6**. e28606.

Craft, J. M., Harris, J. A., Hyman, S., Kner, P. and Lechtreck, K. F. (2015). Tubulin transport by IFT is upregulated during ciliary growth by a cilium-autonomous mechanism. *J. Cell Biol.* **208**, 223-237.

Cuschieri, A. and Bannister, L. H. (1975). The development of the olfactory mucosa in the mouse: light microscopy. *J. Anat.* **119**, 277-286.

Domire, J. S., Green, J. A., Lee, K. G., Johnson, A. D., Askwith, C. C. and Mykytyn, K. (2011). Dopamine receptor 1 localizes to neuronal cilia in a dynamic process that requires the Bardet-Biedl syndrome proteins. *Cell. Mol. Life Sci.* **68**, 2951-2960.

Eguether, T., SanAgustin, J. T., Keady, B. T., Jonassen, J. A., Liang, Y., Francis, R., Tobita, K., Johnson, C. A., Abdelhamed, Z. A., Lo, C. W. et al. (2014). IFT27 links the bbsome to ift for maintenance of the ciliary signaling compartment. *Dev. Cell* **31**, 279-290.

Ehrlich, M. E., Grillo, M., Joh, T. H., Margolis, F. L. and Baker, H. (1990). Transneuronal regulation of neuronal specific gene expression in the mouse olfactory bulb. *Brain Res. Mol. Brain Res.* **7**, 115-122.

Engel, B. D., Ludington, W. B. and Marshall, W. F. (2009). Intraflagellar transport particle size scales inversely with flagellar length: Revisiting the balance-point length control model. *J. Cell Biol* **187**, 81-89.

Gascue, C., Tan, P. L., Cardenas-Rodriguez, M., Libisch, G., Fernandez-Calero, T., Liu, Y. P., Astrada, S., Robello, C., Naya, H., Katsanis, N. et al. (2012). Direct role of Bardet-Biedl syndrome proteins in transcriptional regulation. *J. Cell Sci.* **125**, 362-375.

Gerdes, J. M., Liu, Y., Zaghloul, N. A., Leitch, C. C., Lawson, S. S., Kato, M., Beachy, P. A., Beales, P. L., DeMartino, G. N., Fisher, S. et al. (2007). Disruption of the basal body compromises proteasomal function and perturbs intracellular Wnt response. *Nat. Genet.* **39**, 1350-1360.

Green, W. W., Uytingco, C. R., Ukhanov, K., Kolb, Z., Moretta, J., McIntyre, J. C. and Martens, J. R. (2018). Peripheral gene therapeutic rescue of an olfactory ciliopathy restores sensory input, axonal pathfinding, and odor-guided behavior. *J. Neurosci.* **38**, 7462-7475.

Haycraft, C. J., Zhang, Q., Song, B., Jackson, W. S., Detloff, P. J., Serra, R. and Yoder, B. K. (2007). Intraflagellar transport is essential for endochondral bone formation. *Development* **134**, 307-316.

Heon, E., Kim, G., Qin, S., Garrison, J. E., Tavares, E., Vincent, A., Nuangchamnong, N., Anthony Scott, C., Slusarski, D. C. and Sheffield, V. C. (2016). Mutations in C8ORF37 cause Bardet Biedl syndrome (BBS21). *Hum. Mol. Genet.* **25**, 2283-2294.

Iannaccone, A., Mykytyn, K., Persico, A. M., Searby, C. C., Baldi, A., Jablonski, M. M. and Sheffield, V. C. (2005). Clinical evidence of decreased olfaction in Bardet-Biedl syndrome caused by a deletion in the BBS4 gene. *Am. J. Med. Genet.* **132 A**, 343-346.

Jenkins, P. M., Hurd, T. W., Zhang, L., McEwen, D. P., Brown, R. L., Margolis, B., Verhey, K. J. and Martens, J. R. (2006). Ciliary targeting of olfactory CNG channels requires the CNGB1b subunit and the kinesin-2 motor protein, KIF17. *Curr. Biol.* **16**, 1211-1216.

Jenkins, P. M., Mcewen, D. P. and Martens, J. R. (2009). Olfactory cilia: linking sensory cilia function and human disease. *Chem. Senses* **34**, 451-464.

Jin, H., White, S. R., Shida, T., Schulz, S., Aguiar, M., Gygi, S. P., Bazan, J. F. and Nachury, M. V. (2010). The conserved bardet-biedl syndrome proteins assemble a coat that traffics membrane proteins to Cilia. *Cell* **141**, 1208-1219.

Joiner, A. M., Green, W. W., McIntyre, J. C., Allen, B. L., Schwob, J. E. and Martens, J. R. (2015). Primary cilia on horizontal basal cells regulate regeneration of the olfactory epithelium. *J. Neurosci.* **35**, 13761-13772.

Khan, A. O., Decker, E., Bachmann, N., Bolz, H. J. and Bergmann, C. (2016). C8orf37 is mutated in Bardet-Biedl syndrome and constitutes a locus allelic to non-syndromic retinal dystrophies. *Ophthalmic Genet.* **37**, 290-293.

Kim, J. C., Badano, J. L., Sibold, S., Esmail, M. A., Hill, J., Hoskins, B. E., Leitch, C. C., Venner, K., Ansley, S. J., Ross, A. J. et al. (2004). The Bardet-Biedl protein BBS4 targets cargo to the pericentriolar region and is required for microtubule anchoring and cell cycle progression. *Nat. Genet.* **36**, 462-470.

Kulaga, H. M., Leitch, C. C., Eichers, E. R., Badano, J. L., Lesemann, A., Hoskins, B. E., Lupski, J. R., Beales, P. L., Reed, R. R. and Katsanis, N. (2004). Loss of BBS proteins causes anosmia in humans and defects in olfactory cilia structure and function in the mouse. *Nat. Genet.* **36**, 994-998.

Lechtreck, K. F. (2015). IFT-Cargo Interactions and Protein Transport in Cilia. *Trends Biochem. Sci.* **40**, 765-778.

Lechtreck, K.-F., Johnson, E. C., Sakai, T., Cochran, D., Ballif, B. A., Rush, J., Pazour, G. J., Ikebe, M. and Witman, G. B. (2009). The Chlamydomonas reinhardtii BBSome is an IFT cargo required for export of specific signaling proteins from flagella. *J. Cell Biol.* **187**, 1117-1132.

Lechtreck, K. F., Gould, T. J. and Witman, G. B. (2013). Flagellar central pair assembly in Chlamydomonas reinhardtii. *Cilia* **2**, 15.

Leitch, C. C. and Zaghloul, N. A. (2014). BBS4 is necessary for ciliary localization of TrkB receptor and activation by BDNF. *PLoS One* **9**, e98687.

Li, J., Ishii, T., Feinstein, P. and Mombaerts, P. (2004). Odorant receptor gene choice is reset by nuclear transfer from mouse olfactory sensory neurons. *Nature* **428**, 393-399.
Liew, G. M., Ye, F., Nager, A. R., Murphy, J. P., Lee, J. S., Aguiar, M., Breslow, D. K., Gygi, S. P. and Nachury, M. V. (2014). The intraflagellar transport protein ift27 promotes bbsome exit from cilia through the gtpase ARL6/BBS3. *Dev. Cell* **31**, 265-278.
Lindstrand, A., Frangakis, S., Carvalho, C. M. B., Richardson, E. B., McFadden, K. A., Willer, J. R., Pehlivan, D., Liu, P., Pediaditakis, I. L., Sabo, A. et al. (2016). Copy-number variation contributes to the mutational load of bardet-biedl syndrome. *Am. J. Hum. Genet.* **99**, 318-336.
Liu, P. and Lechtreck, K. F. (2018). The Bardet-Biedl syndrome protein complex is an adapter expanding the cargo range of intraflagellar transport trains for ciliary export. *Proc. Natl. Acad. Sci. USA* **115**, E934-E943.
Loktev, A. V. and Jackson, P. K. (2013). Neuropeptide Y family receptors traffic via the bardet-biedl syndrome pathway to signal in neuronal primary cilia. *Cell Rep.* **5**, 1316-1329.
Loktev, A. V., Zhang, Q., Beck, J. S., Searby, C. C., Scheetz, T. E., Bazan, J. F., Slusarski, D. C., Sheffield, V. C., Jackson, P. K. and Nachury, M. V. (2008). A BBSome subunit links ciliogenesis, microtubule stability, and acetylation. *Dev. Cell* **15**, 854-865.
Marshall, W. F. (2008). Chapter 1 basal bodies. platforms for building cilia. *Curr. Top. Dev. Biol.* **85**, 1-22.
May-Simera, H. L., Ross, A., Rix, S., Forge, A., Beales, P. L. and Jagger, D. J. (2009). Patterns of expression of Bardet-Biedl syndrome proteins in the mammalian cochlea suggest noncentrosomal functions. *J. Comp. Neurol.* **514**, 174-188.
McIntyre, J. C., Davis, E. E., Joiner, A., Williams, C. L., Tsai, I.-C., Jenkins, P. M., McEwen, D. P., Zhang, L., Escobado, J., Thomas, S. et al. (2012). Gene therapy rescues cilia defects and restores olfactory function in a mammalian ciliopathy model. *Nat. Med.* **18**, 1423-1428.
Menco, M. (1980). Qualitative and quantitative freeze-fracture studies on olfactory and nasal respiratory epithelial surfaces of frog, ox, rat, and dog - II. Cell apices, cilia, and microvilli. *Cell Tissue Res.* **211**, 5-29.
Menco, B. P. and Farbman, A. I. (1985). Genesis of cilia and microvilli of rat nasal epithelia during pre-natal development. I. Olfactory epithelium, qualitative studies. *J. Cell Sci.* **78**, 283-310.
Michalakis, S., Reisert, J., Geiger, H., Wetzel, C., Zong, X., Bradley, J., Spehr, M., Hüttl, S., Gerstner, A., Pfeifer, A. et al. (2006). Loss of CNGB1 protein leads to olfactory dysfunction and subciliary cyclic nucleotide-gated channel trapping. *J. Biol. Chem.* **281**, 35156-35166.
Miyoshi, K., Kasahara, K., Miyazaki, I., Shimizu, S., Taniguchi, M., Matsuzaki, S., Tohyama, M. and Asanuma, M. (2009). Pericentrin, a centrosomal protein related to microcephalic primordial dwarfism, is required for olfactory cilia assembly in mice. *FASEB J.* **23**, 3289-3297.
Mokrzan, E. M., Lewis, J. S. and Mykytyn, K. (2007). Differences in renal tubule primary cilia length in a mouse model of Bardet-Biedl syndrome. *Nephron - Exp. Nephrol.* **106**, e88-e96.
Mykytyn, K., Braun, T., Carmi, R., Haider, N. B., Searby, C. C., Shastri, M., Beck, G., Wright, A. F., Iannaccone, A., Elbedour, K. et al. (2001). Identification of the gene that, when mutated, causes the human obesity syndrome BBS4. *Nat. Genet.* **28**, 188-191.
Mykytyn, K., Mullins, R. F., Andrews, M., Chiang, A. P., Swiderski, R. E., Yang, B., Braun, T., Casavant, T., Stone, E. M. and Sheffield, V. C. (2004). Bardet-Biedl syndrome type 4 (BBS4)-null mice implicate Bbs4 in flagella formation but not global cilia assembly. *Proc. Natl. Acad. Sci. USA* **101**, 8664-8669.
Nachury, M. V., Loktev, A. V., Zhang, Q., Westlake, C. J., Peränen, J., Merdes, A., Slusarski, D. C., Scheller, R. H., Bazan, J. F., Sheffield, V. C. et al. (2007). A core complex of BBS proteins cooperates with the GTPase Rab8 to promote ciliary membrane biogenesis. *Cell* **129**, 1201-1213.
Nager, A. R., Goldstein, J. S., Herranz-Pérez, V., Portran, D., Ye, F., Garcia-Verdugo, J. M. and Nachury, M. V. (2017). An actin network dispatches ciliary GPCRs into extracellular vesicles to modulate signaling. *Cell* **168**, 252-263.e14.
Nishimura, D. Y., Fath, M., Mullins, R. F., Searby, C., Andrews, M., Davis, R., Andorf, J. L., Mykytyn, K., Swiderski, R. E., Yang, B. et al. (2004). Bbs2-null mice have neurosensory deficits, a defect in social dominance, and retinopathy associated with mislocalization of rhodopsin. *Proc. Natl. Acad. Sci. USA* **101**, 16588-16593.
Ou, G., Blacque, O. E., Snow, J. J., Leroux, M. R. and Scholey, J. M. (2005). Functional coordination of intraflagellar transport motors. *Nature* **436**, 583-587.
Pan, X., Ou, G., Civelekoglu-Scholey, G., Blacque, O. E., Endres, N. F., Tao, L., Mogilner, A., Leroux, M. R., Vale, R. D. and Scholey, J. M. (2006). Mechanism of transport of IFT particles in C. elegans cilia by the concerted action of kinesin-II and OSM-3 motors. *J. Cell Biol.* **174**, 1035-1045.
Pearson, C. G. and Winey, M. (2009). Basal body assembly in ciliates: the power of numbers. *Traffic* **10**, 461-471.
Pearson, C. G., Giddings, T. H., Jr. and Winey, M. (2009). Basal body components exhibit differential protein dynamics during nascent basal body assembly. *Mol. Biol. Cell* **20**, 904-914.
Picariello, T., Valentine, M. S., Yano, J. and Van Houten, J. (2014). Reduction of meckelin leads to general loss of cilia, ciliary microtubule misalignment and distorted cell surface organization. *Cilia* **3**, 2.
Pigino, G., Geimer, S., Lanzavecchia, S., Paccagnini, E., Cantele, F., Diener, D. R., Rosenbaum, J. L. and Lupetti, P. (2009). Electron-tomographic analysis of intraflagellar transport particle trains in situ. *J. Cell Biol* **187**, 135-148.
Prieto-Echagüe, V., Lodh, S., Colman, L., Bobba, N., Santos, L., Katsanis, N., Escande, C., Zaghloul, N. A. and Badano, J. L. (2017). BBS4 regulates the expression and secretion of FSTL1, a protein that participates in ciliogenesis and the differentiation of 3T3-L1. *Sci. Rep.* **7**, **7**, 9765.
Reiter, J. F. and Leroux, M. R. (2017). Genes and molecular pathways underpinning ciliopathies. *Nat. Rev. Mol. Cell Biol.* **18**, 533-547.
Riise, R., Tornqvist, K., Wright, A. F., Mykytyn, K. and Sheffield, V. C. (2002). The phenotype in Norwegian patients with Bardet-Biedl syndrome with mutations in the BBS4 gene. *Arch. Ophthalmol.* **120**, 1364-1367.
Rosenbaum, J. L. and Witman, G. B. (2002). Intraflagellar transport. *Nat. Rev. Mol. Cell Biol.* **3**, 813-825.
Sánchez, I. and Dynlacht, B. D. (2016). Cilium assembly and disassembly. *Nat. Cell Biol.* **18**, 711-717.
Scheidecker, S., Etard, C., Pierce, N. W., Geoffroy, V., Schaefer, E., Muller, J., Chennen, K., Flori, E., Pelletier, V., Poch, O. et al. (2014). Exome sequencing of Bardet-Biedl syndrome patient identifies a null mutation in the bbsome subunit BBIP1 (BBS18). *J. Med. Genet.* **51**, 132-136.
Schwob, J. E., Jang, W., Holbrook, E. H., Lin, B., Herrick, D. B., Peterson, J. N. and Hewitt Coleman, J. (2017). Stem and progenitor cells of the mammalian olfactory epithelium: taking poietic license. *J. Comp. Neurol.* **525**, 1034-1054.
Seo, S., Guo, D.-F., Bugge, K., Morgan, D. A., Rahmouni, K. and Sheffield, V. C. (2009). Requirement of Bardet-Biedl syndrome proteins for leptin receptor signaling. *Hum. Mol. Genet.* **18**, 1323-1331.
Seo, S., Zhang, Q., Bugge, K., Breslow, D. K., Searby, C. C., Nachury, M. V. and Sheffield, V. C. (2011). A novel protein LZTFL1 regulates ciliary trafficking of the BBSome and smoothened. *PLoS Genet.*. **7**, e1002358.
Shah, A. S., Farmen, S. L., Moninger, T. O., Businga, T. R., Andrews, M. P., Bugge, K., Searby, C. C., Nishimura, D., Brogden, K. A., Kline, J. N. et al. (2008). Loss of Bardet-Biedl syndrome proteins alters the morphology and function of motile cilia in airway epithelia. *Proc. Natl. Acad. Sci. USA* **105**, 3380-3385.
Snow, J. J., Ou, G., Gunnarson, A. L., Walker, M. R. S., Zhou, H. M., Brust-Mascher, I. and Scholey, J. M. (2004). Two anterograde intraflagellar transport motors cooperate to build sensory cilia on C. elegans neurons. *Nat. Cell Biol.* **6**, 1109-1113.
Starks, R. D., Beyer, A. M., Guo, D. F., Boland, L., Zhang, Q., Sheffield, V. C. and Rahmouni, K. (2015). Regulation of insulin receptor trafficking by Bardet Biedl syndrome proteins. *PLoS Genet.*. **11**, e1005311.
Stawicki, T. M., Hernandez, L., Esterberg, R., Linbo, T., Owens, K. N., Shah, A. N., Thapa, N., Roberts, B., Moens, C. B., Rubel, E. W. et al. (2016). Cilia-associated genes play differing roles in aminoglycoside-induced hair cell death in zebrafish. *G3 & Genes|Genomes|Genetics* **6**, 2225-2235.
Stepanek, L. and Pigino, G. (2016). Microtubule doublets are double-track railways for intraflagellar transport trains. *Science* **352**, 721-724.
Swiderski, R. E., Agassandian, K., Ross, J. L., Bugge, K., Cassell, M. D. and Yeaman, C. (2012). Structural defects in cilia of the choroid plexus, subfornical organ and ventricular ependyma are associated with ventriculomegaly. *Fluids Barriers CNS* **9**, 22.
Tadenev, A. L. D., Kulaga, H. M., May-Simera, H. L., Kelley, M. W., Katsanis, N. and Reed, R. R. (2011). Loss of Bardet-Biedl syndrome protein-8 (BBS8) perturbs olfactory function, protein localization, and axon targeting. *Proc. Natl. Acad. Sci. USA* **108**, 10320-10325.
Vannuccini, E., Paccagnini, E., Cantele, F., Gentile, M., Dini, D., Fino, F., Diener, D., Mencarelli, C. and Lupetti, P. (2016). Two classes of short intraflagellar transport train with different 3D structures are present in *Chlamydomonas* flagella. *J. Cell Sci* **129**, 2064-2074.
Wang, Z. and Storm, D. R. (2006). Extraction of DNA from mouse tails. *BioTechniques* **41**, 410-412.
Wang, L., Lee, K., Malonis, R., Sanchez, I. and Dynlacht, B. D. (2016). Tethering of an E3 ligase by PCM1 regulates the abundance of centrosomal KIAA0586/Talpid3 and promotes ciliogenesis. *Elife* **5**, e12950.
Wei, Q., Zhang, Y., Li, Y., Zhang, Q., Ling, K. and Hu, J. (2012). The BBSome controls IFT assembly and turnaround in cilia. *Nat. Cell Biol.* **14**, 950-957.
Williams, C. L., McIntyre, J. C., Norris, S. R., Jenkins, P. M., Zhang, L., Pei, Q., Verhey, K. and Martens, J. R. (2014). Direct evidence for BBSome-associated intraflagellar transport reveals distinct properties of native mammalian cilia. *Nat. Commun.* **5**, 5813.
Williams, C. L., Uytingco, C. R., Green, W. W., McIntyre, J. C., Ukhanov, K., Zimmerman, A. D., Shively, D. T., Zhang, L., Nishimura, D. Y., Sheffield, V. C. et al. (2017). Gene therapeutic reversal of peripheral olfactory impairment in Bardet-Biedl syndrome. *Mol. Ther.* **25**, 904-916.
Wren, K. N., Craft, J. M., Tritschler, D., Schauer, A., Patel, D. K., Smith, E. F., Porter, M. E., Kner, P. and Lechtreck, K. F. (2013). A differential cargo-loading model of ciliary length regulation by IFT. *Curr. Biol.* **23**, 2463-2471.
Xu, Q., Zhang, Y., Wei, Q., Huang, Y., Li, Y., Ling, K. and Hu, J. (2015). BBS4 and BBS5 show functional redundancy in the BBSome to regulate the degradative sorting of ciliary sensory receptors. *Sci. Rep.* **5**, 11855.

Ye, F., Nager, A. R. and Nachury, M. V. (2018). BBSome trains remove activated GPCRs from cilia by enabling passage through the transition zone. *J. Cell Biol.* **217**, 1847-1868.

Ying, G., Avasthi, P., Irwin, M., Gerstner, C. D., Frederick, J. M., Lucero, M. T. and Baehr, W. (2014). Centrin 2 is required for mouse olfactory ciliary trafficking and development of ependymal cilia planar polarity. *J. Neurosci.* **34**, 6377-6388.

Zacharias, D. A., Violin, J. D., Newton, A. C. and Tsien, R. Y. (2002). Partitioning of lipid-modified monomeric GFPs into membrane microdomains of live cells. *Science* **296**, 913-916.

Zhang, Q., Yu, D., Seo, S., Stone, E. M. and Sheffield, V. C. (2012). Intrinsic protein-protein interaction-mediated and chaperonin-assisted sequential assembly of stable Bardet-Biedl syndrome protein complex, the BBSome. *J. Biol. Chem.* **287**, 20625-20635.

Zheng, C., Feinstein, P., Bozza, T., Rodriguez, I. and Mombaerts, P. (2000). Peripheral olfactory projections are differentially affected in mice deficient in a cyclic nucleotide-gated channel subunit. *Neuron* **26**, 81-91.

Zou, D.-J., Chesler, A. T., Le Pichon, C. E., Kuznetsov, A., Pei, X., Hwang, E. L. and Firestein, S. (2007). Absence of adenylyl cyclase 3 perturbs peripheral olfactory projections in mice. *J. Neurosci.* **27**, 6675-6683.